POLITECNICO DI TORINO
Repository ISTITUZIONALE

Experimental Investigation of the Mooring System of a Wave Energy Converter in Operating and Extreme Wave Conditions

Original
Experimental Investigation of the Mooring System of a Wave Energy Converter in Operating and Extreme Wave Conditions / Sirigu, S.A., Bonfanti, M., Begovic, E., Bertorello, C., Dafnakis, P., Giorgi, G., Bracco, G., Mattiazzo, G.. - In: JOURNAL OF MARINE SCIENCE AND ENGINEERING. - ISSN 2077-1312. - 8:3(2020), p. 180. [10.3390/jmse8030180]

Availability:
This version is available at: 11583/2807556 since: 2021-06-25T18:04:51Z

Publisher:
MDPI

Published
DOI:10.3390/jmse8030180

Terms of use:

This article is made available under terms and conditions as specified in the corresponding bibliographic description in the repository

Publisher copyright

(Article begins on next page)

25 November 2026

Journal of
Marine Science and Engineering

MDPI

Article

Experimental Investigation of the Mooring System of a Wave Energy Converter in Operating and Extreme Wave Conditions

Sergej Antonello Sirigu [1,*], Mauro Bonfanti [1], Ermina Begovic [2], Carlo Bertorello [2], Panagiotis Dafnakis [1], Giuseppe Giorgi [1], Giovanni Bracco [1] and Giuliana Mattiazzo [1]

[1] Department of Mechanical and Aerospace Engineering, Polytechnic of Turin, C.so Duca degli Abruzzi, 24, 10129 Turin, Italy; mauro.bonfanti@polito.it (M.B.); panagiotis.dafnakis@polito.it (P.D.); giuseppe.giorgi@polito.it (G.G.); giovanni.bracco@polito.it (G.B.); giuliana.mattiazzo@polito.it (G.M.)

[2] Department of Industrial Engineering, University of Naples Federico II, Via Claudio, 21, 80125 Naples, Italy; begovic@unina.it (E.B.); bertorel@unina.it (C.B.)

* Correspondence: sergej.sirigu@polito.it

Received: 13 February 2020; Accepted: 4 March 2020; Published: 7 March 2020



Abstract: A proper design of the mooring systems for Wave Energy Converters (WECs) requires an accurate investigation of both operating and extreme wave conditions. A careful analysis of these systems is required to design a mooring configuration that ensures station keeping, reliability, maintainability, and low costs, without affecting the WEC dynamics. In this context, an experimental campaign on a 1:20 scaled prototype of the ISWEC (Inertial Sea Wave Energy Converter), focusing on the influence of the mooring layout on loads in extreme wave conditions, is presented and discussed. Two mooring configurations composed of multiple slack catenaries with sub-surface buoys, with or without clump-weights, have been designed and investigated experimentally. Tests in regular, irregular, and extreme waves for a moored model of the ISWEC device have been performed at the University of Naples Federico II. The aim is to identify a mooring solution that could guarantee both correct operation of the device and load carrying in extreme sea conditions. Pitch motion and loads in the rotational joint have been considered as indicators of the device hydrodynamic behavior and mooring configuration impact on the WEC.

Keywords: mooring system; wave energy converter; experimental campaign; floating WEC mooring design; operating conditions; extreme conditions

1. Introduction

Although mooring technologies employed for Wave Energy Converters are based on the offshore Oil&Gas industry experience and solutions [1], the marine energy sector presents specific requirements and several additional challenges [2]. Each wave energy device requires a specific design study for the mooring system, which is influenced by its energy extraction method, determining the most suitable solution [3]. As highlighted in [4,5], wave energy converters are commonly designed and studied by numerical models previously used in the offshore engineering industry. As stated by [6], the main advantages of the numerical simulations over the experimental tests of real WEC prototypes are the significant costs and time reduction during the conceptual design stage. However, there is a drawback in accuracy of the computationally cheap numerical methods due to the assumption of linear phenomena, assuming small amplitude of the dynamic response of floater in low steepness waves, static wetted surface, and linearized free surface boundary conditions. In this regard, when developing a WEC, it is fundamental to rely on experimental analyses, theoretical studies, and experience obtained from real prototype function in the open sea. In particular, the mooring system is considered a vital

part of a WEC design because it influences the dynamics of the device and accounts for a significant proportion of the project's overall capital cost [7].

The design phase and survivability analyses of a WEC crucially require accurate numerical modeling, in synergy with the experimental investigation of the hydrodynamic loads acting on the device [8]. In [9], the experimental results of a 1:20 model scale of oscillating water column (OWC), installed as a prototype in Galway Bay, are reported. The device was tested with three different mooring chain lengths in regular and irregular waves, corresponding to the accidental limit state (ALS) and to extreme conditions. The authors reported that the stiff mooring configuration (the shortest chain length) might be preferable for both the limitation of the drift and of the force on the chain/rope in the severe wave conditions. An experimental investigation on the behavior of a taut-mooring system of a floating WEC can be found in [10]. The mooring system was designed so that its extension was insufficient to fully accommodate the waves under consideration, hence generating extreme loads in the mooring line and anchor. Such extreme loads, generated by focused wave, represent a worst-case scenario, which such experiments purported to investigate. Important conclusions of this work are that the wave steepness has only a minor effect on the magnitude of the initial snatch loads; on the other hand, for a dynamically responding floating body, mooring loads are dependent on the displacement history. Furthermore, a single focused wave cannot be used to obtain an accurate assessment of extreme mooring loads. An experimental study of the benefits and the impacts that different mooring concepts might have on point absorbers can be found in [11]. Authors tested three different configurations: (i) compact (small seabed footprint) configuration consisting of a synthetic cable and a floater; (ii) a compact configuration composed of a synthetic cable, a floater and a clump-weight in a zig–zag geometry; and (iii) a catenary, as the industry standard solution. In particular, the configuration with a floater and a clump weight had a slightly worse performance than the one with only the floater, as far as power extraction is concerned. However, configuration (ii) was the best at keeping the cables under tension while minimizing the dynamic tension. Moreover, the configuration with a floater and a clump-weight had the smallest impact on the natural period of the pitch mode of motion. An experimental research on a 1:25 scaled floating OWC WEC model can be found in [12]. Two types of mooring materials were considered: an iron chain and a nylon rope have been used, investigating their influence on the tension in mooring lines. Authors concluded that the soft nylon rope can introduce significantly larger surge motion; for the iron chain configuration, no shock loads were observed in the tested wave conditions.

In this paper, the experimental testing campaign of the 1:20 model scale of ISWEC (Inertial Sea Wave Energy Converter) prototype and its specifically designed mooring layout is presented. ISWEC is a floating device developed in Polytechnic of Turin, Italy. The device converts the energy of the incoming wave through a gyroscopic unit working in resonant conditions with the sea state. The power extraction performance is directly linked to the pitch motion of the floater [13]. In this regard, the design of the ISWEC mooring system should not affect the pitching motion in operational conditions, and it has to guarantee the station keeping in extreme wave conditions. This paper focuses on the design of two mooring configurations and the experimental investigation of their influence on the hydrodynamic performances of the ISWEC device. A slack mooring layout based on chain lines is presented, and the effect of introducing clump weights on the mooring lines is evaluated. The proposed mooring systems were designed to have lower mooring loads impact during the operational sea state conditions and to guarantee the survivability of the device in extreme sea state conditions.

Although slack mooring systems with submerged buoys and clump weights are common in the traditional ocean engineering field, wave energy applications require a different design in order to withstand extreme loads while guaranteeing efficient operation and power absorption. Slack moorings for wave energy applications are mainly used for axisymmetric buoys working as point absorbers, extracting energy from the heave motion, such as [8,14]. However, thanks to their geometrical symmetry and working principle, such devices are insensitive to the wave direction. The consequence on the mooring system design is that lines are directly attached to the buoy. Conversely, the ISWEC

belongs to the class of pitching platforms and needs to self-align to the main wave direction in order to guarantee efficient operation. However, examples of pitching floating platform WECs are scarce [15,16], compared to more common technologies [17–19]. Therefore, this paper provides a valuable description of a technological solution for passive weathervaning that also guarantees limited influence on the important dynamics for power extraction of a WEC of the pitching platform class. An experimental campaign in regular, irregular, and extreme wave conditions was performed in the towing tank of the Department of Industrial Engineering at University of Naples Federico II, Italy. Pitch motion and loads in the rotational joint have been analyzed as the indicators of the device's hydrodynamic behavior and mooring configuration effect on the WEC.

2. Mooring Solutions for Floating WECs

Mooring systems are constituted by different components, generally composed of anchors, mooring lines, buoys, clump-weights, and connectors. A first distinction can be made between slack and taut mooring systems. On the one hand, slack-moored configurations are typically based on catenary dispositions and mainly rely on the gravity force of the mooring lines to provide the necessary horizontal and vertical restoring forces. On the other hand, the restoring capabilities of taut lines, usually composed of either steel wire or synthetic ropes, are based on the axial stiffness of the lines and need to be pre-tensioned before their operation. Taut mooring systems, although having the advantage of a small footprint, determine a high stiffness that is likely to affect negatively the motion of wave energy devices [20,21]. Furthermore, they require very expensive foundations, as vertically loaded piled anchors [22]. The main mooring system configurations suitable for floating WECs are reported in Figure 1 [23–26]:

- Single Catenary (a): It is the simplest and least expensive configuration. It belongs to the single point mooring systems and its geometry provides a high compliance, resulting in possible large motions of the device and weather-vaning. The horizontal restoring force is provided only by the weight of the chain. The high footprint and compliance are not suitable for arrays of WECs because collisions may occur. Moreover, no redundancy is present in the case of failure.
- Multi-catenary: this configuration allows the sharing of loads among different lines. Redundancy is provided and allowed motions are reduced by the geometry of the system. However, more components are present, resulting in increased costs.
- CALM: In the Catenary Anchor Leg Mooring, a buoy is introduced close to the surface, minimizing the influence on the vertical motions of the WEC. The upward force exerted by the buoyancy increases the restoring capabilities of the system. This system guarantees larger motions with respect to the multi-catenary, reducing the impedance and the damping related to the mooring. The device can weathervane around the buoy, but, on the other hand, being at the water surface, the buoy is subjected to current and wind loading. Likewise, in the multi-catenary system, more components are present, resulting in higher costs.
- Lazy-wave: In this case, the buoy is submerged, and a clump-weight is introduced. This solution provides lower horizontal loads with respect to the CALM system because no taut lines are present. The geometric compliance of the system is thus increased.

Different combinations of the presented configurations can be used for the final design of a mooring system, depending on the specific device of interest.

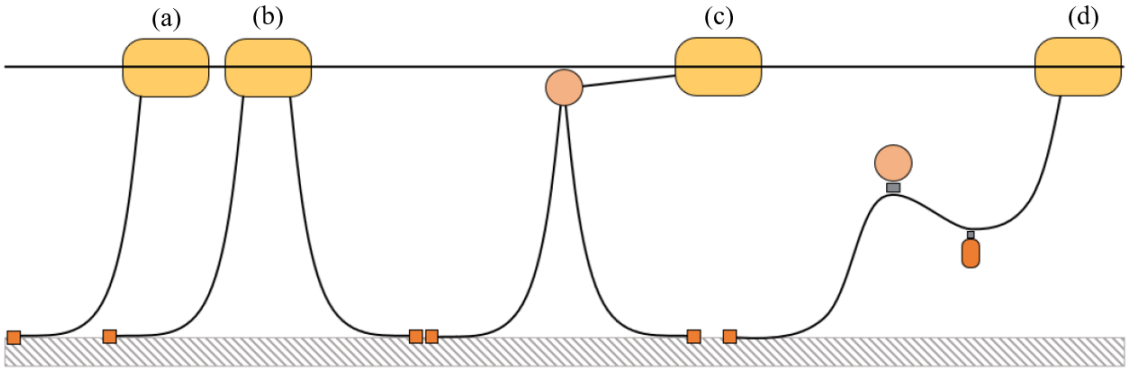

Figure 1. Mooring configurations: (**a**) catenary; (**b**) multi-catenary; (**c**) CALM; (**d**) lazy-wave.

3. ISWEC Device

The first idea of the ISWEC (Inertial Sea Wave Energy Converter) device dates back to the 2006 and has been developed at the Polytechnic of Turin, following different stages from virtual modeling to experimental tests on scale models, as described in [27]. ISWEC is a fully-enclosed floating gyroscopic WEC, especially designed for the Mediterranean Sea [28–31]. The device presented in this paper is the 1 Degree-of-Freedom (DoF) ISWEC, a directional device brought from concept to full scale prototyping in Pantelleria in August 2015 [32]. This floating device is considered as a case study for the analysis of the mooring system presented in this work.

3.1. ISWEC Device

ISWEC is a floating wave energy converter designed to exploit wave energy through the gyroscopic effect of a flywheel [33]. The gyroscopic power take-off (PTO) system is enclosed in a sealed hull [34], retained by slack mooring lines anchored on the seabed. A schematic representation of the device concept is shown in Figure 2. The pitching motion of the floater δ induces a precession oscillation ε of the gyroscope. Extraction of energy from the system is achieved by damping the precession of the gyroscope. The PTO is an electrical torque generator connected to the gyroscope support frame through a gearbox with a gear ratio 1/10. The maximum energy extraction rate is obtained by properly tuning the flywheel spinning speed with the incoming sea state and controlling the PTO torque [35].

The 3D representation of the deployed device is shown in Figure 2, highlighting the relevant subsystems: the Floater, Ballasts in order to tune the natural frequency of the device with respect to a reference/base sea state, and two Gyroscopes. The gyroscope is composed of a spinning Flywheel, driven by the Flywheel motor and supported by a Support structure that allow the flywheel to rotate around both the vertical axis (z_1) and the precession axis (ε). The power extraction is performed by an Electrical generator coupled with the precession axis of the gyroscope.

The derivation of the dynamic model equations for the complete system (hydrodynamics of the hull and PTO equations) is not in the scope of this work and details can be found in [36]. Furthermore, an accurate description of the internal components of the full-scale device and a more detailed discussion on the hull design can be found in [37].

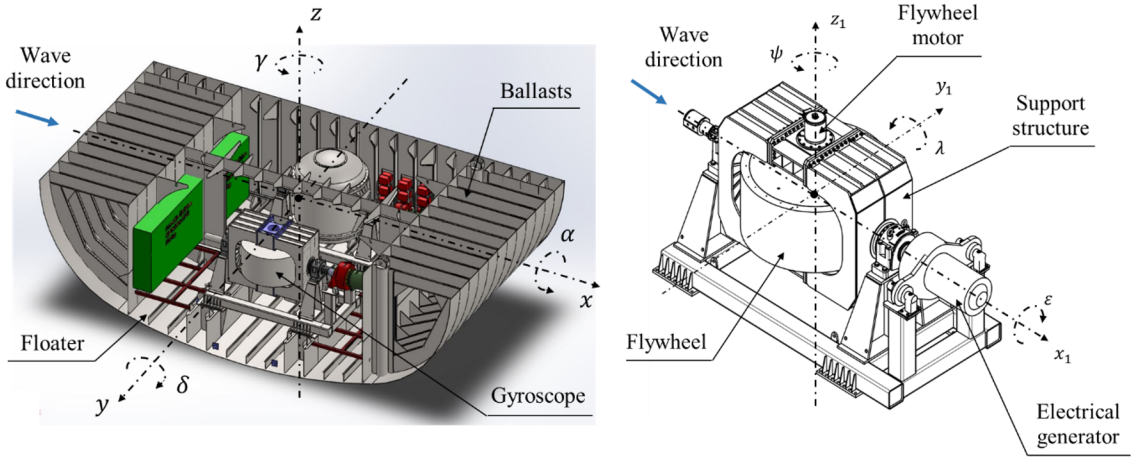

Figure 2. ISWEC full-scale configuration and internal components (**left**); ISWEC gyroscope (**right**).

3.2. ISWEC Mooring System

Based on the ISWEC working principle, the mooring system must guarantee the following requirements:

- Station keeping: the device must be maintained within the specified devoted area.
- Electrical cable safeguard: the motion of the device must avoid tension loads in the electrical transmission cable.
- Compliance: to sustain the environmental loads on the device, the mooring lines and the anchors must comply with the classification and regulations imposed by ruling authorities.
- Passive behavior: the mooring system must minimize the disturbance on the device motion appointed to the power conversion chain (i.e., pitch motion). On the contrary, the horizontal motions need to be constrained, limiting the device drift to ensure station keeping.
- Weathervaning: the ISWEC device should always orientate towards the incident wave, to exploit its pitch motion.: the area dedicated to a single device should be minimized, easing a future installation in an array configuration.
- Reduced maintenance: when possible, the use of high durability component is preferred, to minimize maintenance operations over the service life.
- Redundancy: a degree of redundancy is desirable, according to an appropriate cost analysis.

Referring to the different mooring configurations suitable for floating WECs described Section 2, the attention is focused on slack mooring solutions because the ISWEC device of interest has a PTO enclosed in the floater and active moorings are not suitable. Moreover, the mooring forces should not interfere with the pitching motion in operation conditions, since the pitch amplitude of motion is proportional to the harvested power.

The ISWEC mooring system is a slack catenary type—Single Anchor Leg Mooring (SALM) composed of multiple mooring lines. In order to guarantee the weather-vaning of the device in respect to the wave direction, a proper center of rotation of the system needs to be designed. Moreover, the ISWEC has to be connected to the electrical grid with a power transmission connection. The electric cable must move together with the hull, both to avoid the interference between the cable and the mooring lines and to guarantee the correct operation. In this regard, an electrical slip ring and mechanical swivel have been chosen.

DNV standards [38] recommend multiple catenary lines, anchored to the bottom of the sea and connected to the center of the circumference through a mechanical swivel that allows the rotation of the top of the system. The joint includes also an electric slip ring able to transmit power. The ISWEC hull is connected to the swivel by means of two bridles that prevent the roll motion of the device.

The mooring connection points are placed towards the bow, with respect to the center of gravity of the device, in order to guarantee a lever arm that stabilizes the device at yaw and guarantees the alignment. On each of the bottom catenary, a sub-surface buoy is installed to enhance the elastic recall of the system and avoid snatches. As shown in Figure 3, two different mooring systems are considered. The main difference between the configurations C1 and C2 is the existence of a clump weight in each mooring line of layout C2. The purpose of the specific alteration is to increase the mooring stiffness. Figure 4 presents the top view of configuration C2.

The cable is connected to the hull deck by a waterproof connector and steered to the slip ring. At the bottom of the slip ring, the submarine cable is attached. The cable is then connected to the grid submarine cable with a second waterproof connector. The most critical component is the rotating joint, where both electrical and mechanical functions are integrated, which connects the upper and lower parts of the mooring system. It follows that, for the ISWEC mooring system, the loads sustained by the joint are of major concern.

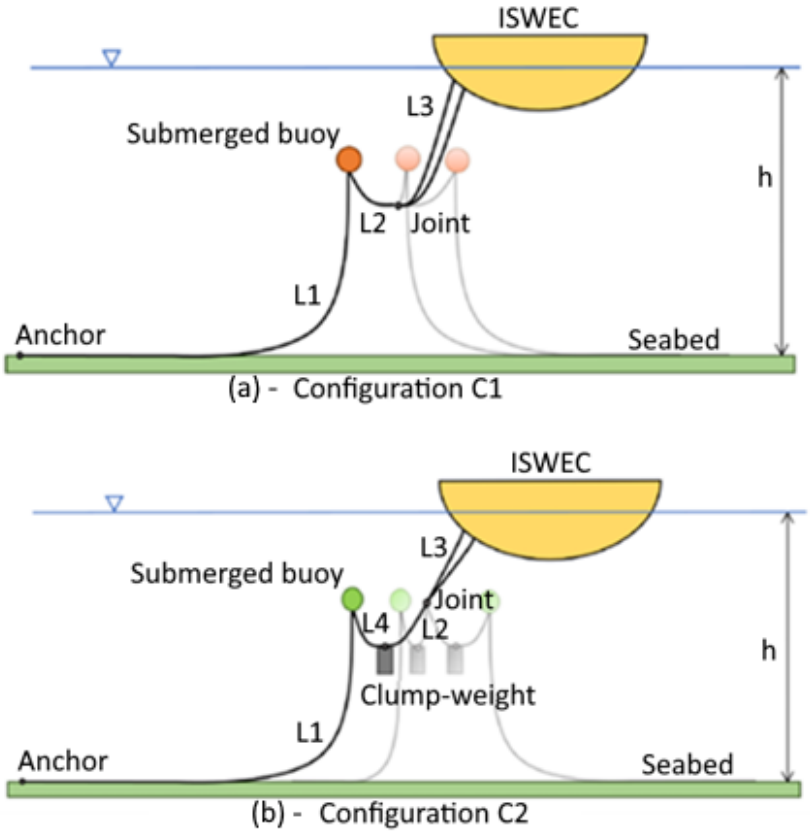

Figure 3. ISWEC mooring layouts: (**a**) C1; (**b**) C2.

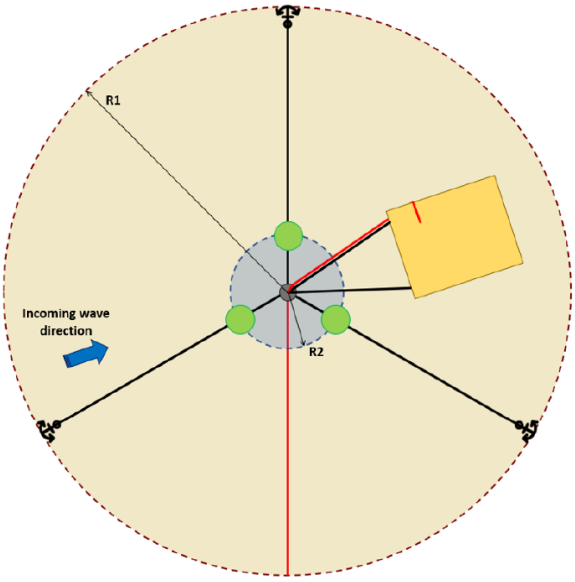

Figure 4. ISWEC mooring layout C2, top view.

4. ISWEC Moored Device Experimental Campaign

The first experimental campaign in regular waves have been performed on the free model [31,39]. This work started from the known pitch Response Amplitude Operator (RAO) and evaluates the performance of the ISWEC mooring configurations, in both operational and extreme wave conditions. The experimental campaign was performed in the towing tank of the University of Naples Federico II, Italy. Furthermore, the effect of the introduction of clump weights (to reduce the loads on the rotating joint) on the hydrodynamic performance of the device has been evaluated.

4.1. Experimental Setup

This section deals with a brief description of the experimental setup of the scaled prototype. A summary of the main characteristics of the device, mooring configurations, acquisition system, and the test tank facility are reported.

The 1:20 ISWEC Physical Model

The ISWEC device was Froude-scaled using a scaling factor of $\lambda = 1/20$. The scale was chosen as appropriate trade-off between the performance of the wave tank and the objective of the tests. The model's hull, shown in Figure 5, is made of 2.5 mm thick stainless-steel sheets, welded together. Profile bars are welded inside the hull, on its perimeter, to create a supporting frame for the steel ballast bars. The ballast is modular in order to guarantee a flexible setup and to achieve the desired mass distribution. The central volume of the hull is left empty for the installation of the sensors and the data acquisition system. The floater is closed with a transparent PoliMethylMethAcrilate (PMMA) sheet in order to simplify visual inspections. No gyroscopic unit was installed on the model. The main properties of the full-scale device deployed in Pantelleria and its 1:20 scaled prototype are summarized in Table 1.

The values of the vertical position of center of gravity (CoG) and moments of inertia around the x- and y-axes were measured using an inertial balance present in the towing tank of University Federico II, as shown in Figure 5, and an accelerometer CrossBow CXL04GP3-R-AL (manufacturer: MEMSIC). Each measurement has been repeated three times and the sampling frequency was 1000 Hz.

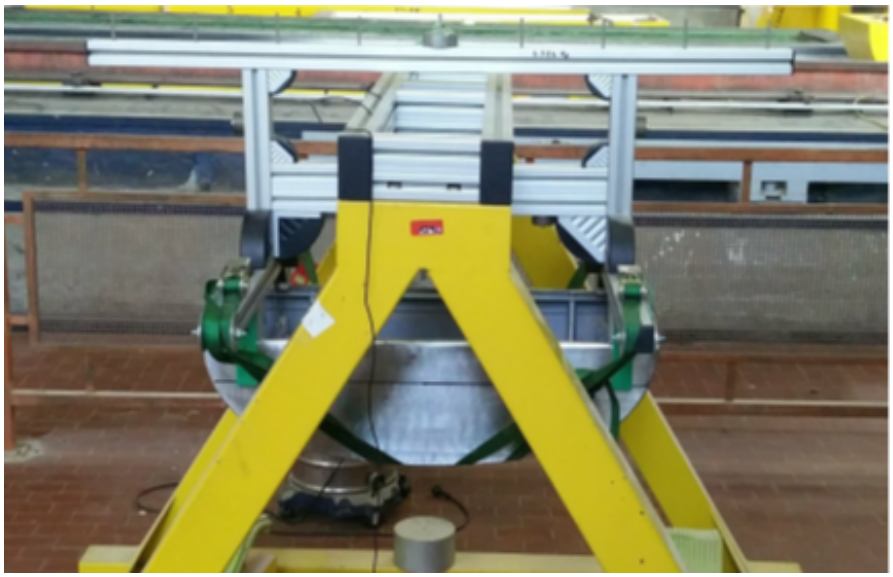

Figure 5. ISWEC center of gravity and moments of inertia and measurement through the inertial balance.

Table 1. ISWEC full-scale and scaled prototype properties.

Parameter	Symbol	Full Scale Model	Scaled Model-TARGET	Experimental Model
Length (m)	L	15.3	0.767	0.767
Beam (m)	B	8	0.400	0.400
Draft (m)	T	3	0.150	0.150
Height (m)	D	4.5	0.225	0.225
Mass (kg)	M	288,090	35.13	35.16
Vertical position of CoG from the bottom (m)	VCG	2.43	0.122	0.120
Roll moment of inertia (kgm^2)	Ixx	1,923,000	0.586	0.775
Pitch moment of inertia (kgm^2)	Iyy	8,486,000	2.587	2.513
Roll radi of inertia (m)	r_{xx}	2.584	0.129	0.149
Pitch moment of inertia (kgm^2)	r_{yy}	5.427	0.271	0.267

It can be noted that the obtained values for radius and moment of inertia in pitch were reproduced within 1.5% and 2.9% difference, respectively. The obtained values for the roll radius and moment of inertia, although reproduced within 7.2 and 15% difference, have been considered acceptable. The difference is mainly due to the position, weight, and dimensions of the measurement equipment installed on board, which are necessary for data acquisition.

Free decay tests were conducted to identify the natural period in the pitch DoF. The objective is the calculation of the damped natural frequency and the identification of linear and quadratic damping of the model, via logarithmic decrease analysis. The methodology used in [40,41] has been chosen as the most effective in this study. Pitch free decay tests were carried out on the free model applying manually an inclination angle with respect to the transverse or longitudinal axis of the hull. After releasing the body, its dynamic response was recorded. Pitch decays have been repeated few times, covering a range of initial angles from 5 to 15 degrees. An example of free decay from 15 deg is shown in Figure 6. The complete set of results for pitch decay is reported in Table 2.

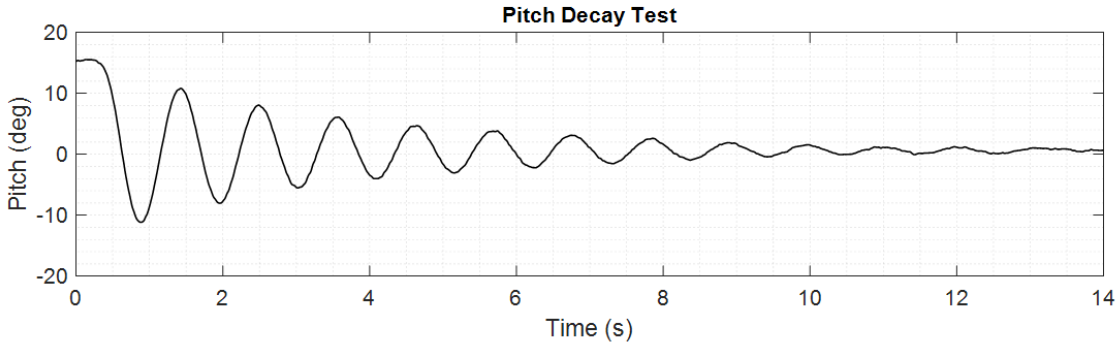

Figure 6. ISWEC pitch decay curve.

Table 2. ISWEC full-scale and scaled prototype properties.

Variable	Symbol	Unit	Model	Full-Scale
Damped natural period	T_{N5}	s	1.070	4.785
Angular coefficient of the regression curve	a	1/s	0.366	-
y-axis intercept of the regression curve	b	1/s	0.242	-
Linear extinction coefficient	α	1/s	0.242	0.054
Quadratic extinction coefficient	β	1/rad	0.147	0.147

4.2. Mooring System

In this experimental campaign, two different mooring configurations have been tested. As shown in Figure 3, the first configuration is the Configuration C1. The second is similar, but a clump-mass is introduced on each of the three mooring bottom lines. The resultant system is a multiple lazy-wave configuration, referred to as Configuration C2. The aim was to test the effect of both submerged buoy and the clump-weight on the restoring force of the mooring system and the load peaks reduction in the dynamic behavior. In addition, a larger clump-mass was further introduced in Configuration C2b, in order to investigate the influence of the mass on the tension peaks. The only differences between configurations C2a and C2b are the net buoyancy of the submerged buoy and the mass of the clump-weight. Configuration C2b is considered only in the extreme wave analysis, discussed in Section 5.3. In Table 3, the main features of the mooring systems considered in the experimental campaign are summarized.

Considering Configuration C2, the gravity force of the clump-mass is chosen to be of the same order of magnitude of the buoyancy force of the submerged buoys. To compensate the sink due to the clump-weight, the submerged buoys volume was increased of the same value from configuration C1 to C2a and C2b. In order to avoid the system from becoming too stiff, another catenary section was added on each line, connecting the submerged buoys to the clump-masses. This section is referred to as L4 and its length must not be small enough to avoid the entanglement of the clump-mass with the bottom catenary. The other catenaries' sections have the same length as in Configuration C1. The same chain diameters were used for both configurations. To ensure a correspondence between the configurations of the moored scale prototype and therefore the scalability of the results, the artificial seabed has been used to correctly emulate the water depth of the installation site. Indeed, the tank water depth is equal to 4.25 m, while a seabed at 1.25 m should be guaranteed.

Table 3. ISWEC mooring system properties, Configuration C1 and C2.

		Configuration C1		Configuration C2a		Configuration C2b	
		Full-Scale	Model	Full-Scale	Model	Full-Scale	Model
Property	**Units**	**Geometry**					
Water depth	m	25	1.25	25	1.25	25	1.25
Anchors Positioning radius	m	60	3	60	3	60	3
L1	m	65	3.25	65	3.25	65	3.25
L2	m	10	0.5	10	0.5	10	0.5
L3	m	10	0.5	10	0.5	10	0.5
L4	m	-	-	5	0.25	5	0.25
Property	**Units**	**Chain properties for bottom mooring lines (L1, L2, and L4)**					
Nominal Diameter	mm	60	3	60	3	60	3
Mass per unit length	kg/m	74.4	0.186	74.4	0.186	74.4	0.186
Mass per unit length in water	kg/m	68.8	0.172	68.8	0.172	68.8	0.172
Proof Load	N	1,940,103	243	1,940,103	243	1,940,103	243
Breaking Load	N	2,770,103	346	2,770,103	346	2,770,103	346
Property	**Units**	**Chain properties for top mooring lines (L3)**					
Nominal Diameter	mm	44	2.2	44	2.2	44	2.2
Mass per unit length	kg/m	36	0.09	36	0.09	36	0.09
Mass per unit length in water	kg/m	32	0.08	32	0.08	32	0.08
Proof Load	N	1,080,103	135	1,080,103	135	1,080,103	135
Breaking Load	N	1,540,103	193	1,540,103	193	1,540,103	193
Property	**Units**	**Submerged buoy and clump mass properties**					
Net buoyancy	kg	1512	0.189	3512	0.439	7042	0.878
Clump mass	kg	-	-	2000	0.25	4000	0.5

The artificial seabed was made using steel bars and PVC (polyvinyl chloride) pipes connected by orthogonal joints in order to create the structure shown in Figure 7. The seabed was built using a flat stretched plastic grid.

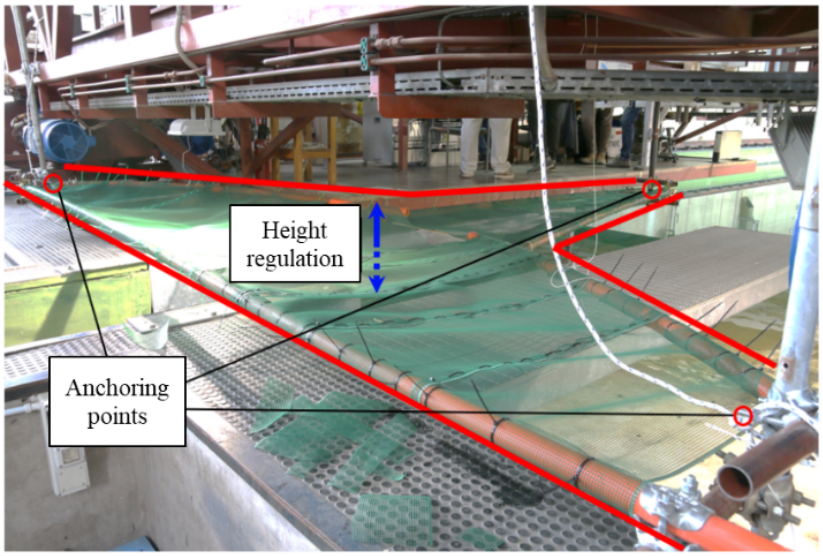

Figure 7. Artificial seabed setup.

Acquisition Systems and Data Management

The scheme of the on-board sensors and their acquisition system is shown in Figure 8. In order to acquire the dynamics of the hull, the floater is equipped with an Inertial Unit of Measurement (IMU) Xsens MTi-30 AHR (manufacturer: Xsens). A National Instrument CompactRIO NI CRIO-9030 (manufacturer: National Instruments) manages the data acquisition, which is a dual core 1.33 GHz real-time control unit. A RS232 serial embedded interface allows for communicating with the MTi unit. The CRIO is equipped with two modules: a NI 9207 Analogue Input module and a NI 9263 Analogue Output module. To monitor and record the mooring tensions along the lines, FUTEK LSB210 is connected on one side to the mechanical swivel and on the other side on both bridle branches. This sensor is submersible and miniaturized in order to not influence the dynamics of the mooring system. A conditioner FUTEK IAA100 is provided and located on-board the device. A Wi-Fi router is connected to the CRIO through an Ethernet embedded interface. Data acquired by the CRIO are transmitted via wireless communication to a remote laptop PC. The DAQ system is powered by a 12 V lead acid battery, installed on board. On the PC host interface, data were visualized in real time and stored with a sampling frequency of f_s = 100 Hz.

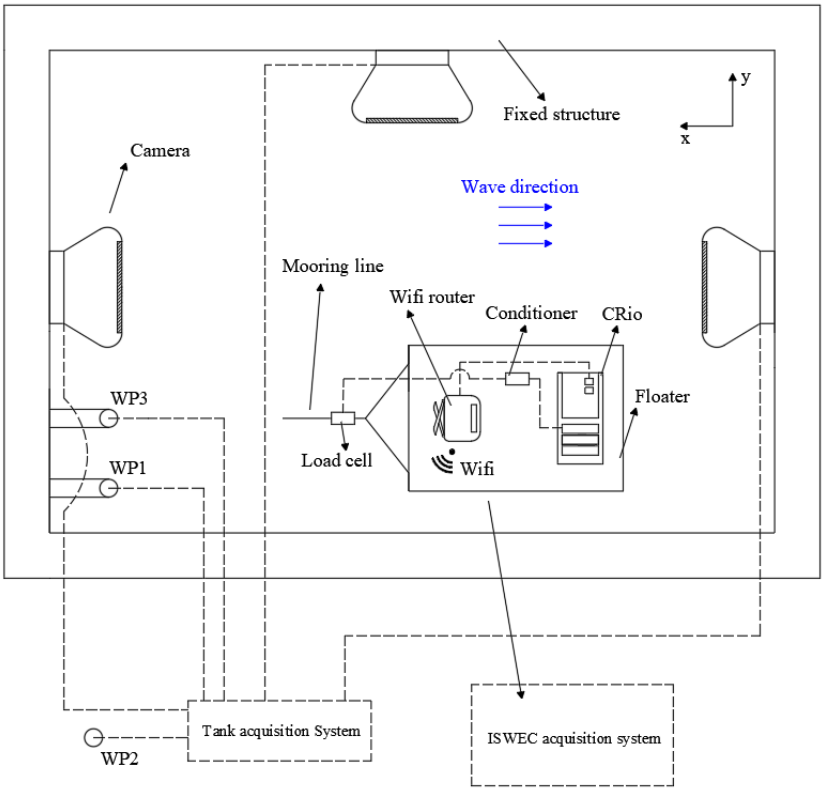

Figure 8. ISWEC prototype and wave tank acquisition system.

In order to guarantee redundancy, a QUALISYS® (Qualsys AB, Göteborg, Sweden) optical motion tracking has captured the device motions. This system tracks the motion of a rigid body through an arrangement of three cameras acquiring the motion of specific reflective markers attached to the body (see Figure 9). The encounter waves are measured by two ultrasonic probes BAUMER UNDK 301U6103/S14 and one capacitive probe AKAMINA AWP-24-3. With reference to Figure 8, the three probes are positioned in such a way as to acquire the wave field at different points to have a redundancy of the measurement. One ultrasonic probe (WP2) is located on the tank side at a lateral distance of 3.96 m from the centerline. The other ultrasonic probe (WP1) and the capacitive probe (WP3) are located at the centerline, 3.215 m ahead of the device CoG. Wave probes and the QUALISYS® motion tracking signals are acquired at a sampling frequency f_s = 500 Hz. These sensors are managed by

the facility's data logging system that provides real-time visualization. The acquired signals from the CRIO and the facility's sensors are synchronized via an analogical trigger signal (0–5 V) generated by the ISWEC on-board CRIO and acquired by the facility's data logging system.

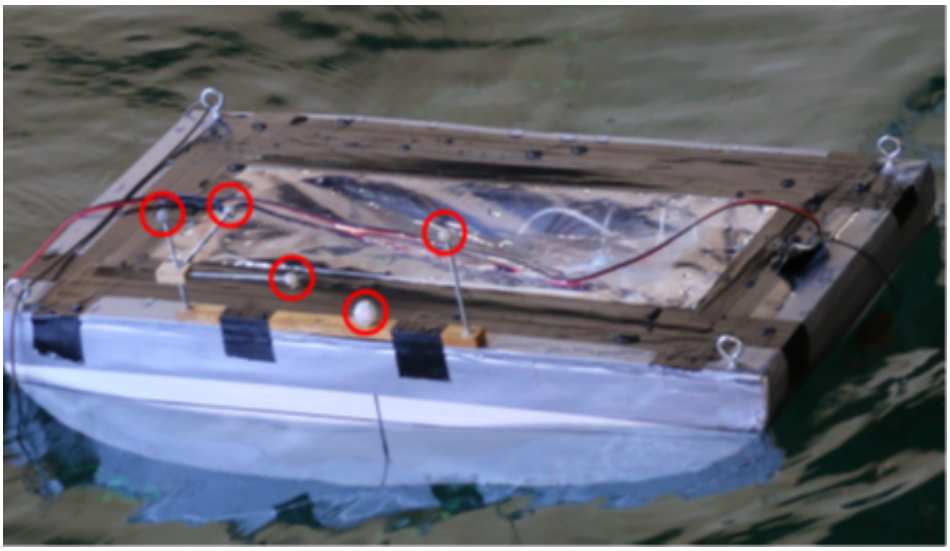

Figure 9. Setup of Qualysis® motion tracking system markers mounted on the device deck.

4.3. Meteocean Data

The installation site of the first full scale prototype of the ISWEC system has been considered for the determination of the environmental loading conditions. The sea site is the harbor of the offshore Pantelleria island, in the northwestern side of the island. The Meteocean analysis was made using two time series from different experimental dataset. The first time series has been obtained from the historical data records of the RON Italian Data Buoy Network [42], choosing a buoy located offshore Mazara del Vallo at 37°26′24″ latitude and 12°32′00″ longitude. The second time series resulted from data acquired at the installation site by a Nortek AWAC acoustic wave gauge [43]. The two datasets were first compared, demonstrating that Mazara del Vallo is very similar to the Pantelleria site. Eventually, the Mazara site dataset was chosen as conservative in terms of safety in the design of the mooring system.

A statistical analysis of the extreme events was performed, aimed at the estimation of the characteristics of the wave properties for specified return periods. From the historical data records of the RON Italian Data Buoy Network [42], it was possible to identify the log-normal probability distribution $p(\chi)$ as the most suitable, having the following form:

$$p(\mathrm{x}) = \frac{1}{\mathrm{x}} \frac{1}{\sigma\sqrt{2\pi}} \exp\left(-\frac{(\ln \mathrm{x} - \mu)^2}{2\sigma^2}\right) \tag{1}$$

where σ is the standard deviation and μ is the expectation of the distribution. From the meteocean data [42], openly available, the best fitting parameters of μ and σ have been identified. From the consequent cumulative distribution function, the properties of the 10- and 100-year return period waves have been determined, shown in Table 4. A JONSWAP spectrum is suitable for the description of the real sea states and a Spectrum Peak Parameter γ = 3.3 was chosen. The results of the spectral properties for the extreme waves are reported in Table 4. The operating conditions measured at the installation site are negligible with respect to the extreme wave conditions. Thus, for this design, only extreme events are considered. As far as operational conditions are concerned, the energetic period of the generated irregular wave was chosen to be close to the pitch resonant period of the floater, and therefore it is representative of the operational condition of the device.

Table 4. Meteocean reference data.

Wave Name	H_s (m)	T_p (s)	γ
Operational wave	2.20	5.41	3.3
10-year wave	5.00	8.70	3.3
100-year wave	5.90	10.30	3.3

4.4. Experimental Tests

All the experimental tests were performed at the towing tank (136.74 m long, 9 m wide, and 4.25 m deep) of the Department of Industrial Engineering of the University Federico II, Naples, Italy. The complete experimental campaign consists of (i) pull-out tests to identify the static characteristics of the mooring system, (ii) regular and (iii) irregular waves analysis to compare the hydrodynamic performances of the floater with the different mooring configurations, and (iv) extreme waves tests to assess the mooring loads in survival wave conditions. All tests were performed by scaling down the waves according to Froude-scale, using a scale factor λ of 1/20, with reference to the meteocean data. All wave tests are performed with the artificial bottom and the model placed in the middle of the tank at 60 m from the wave maker.

Experimental results are also compared with predictions according to numerical models. The potential flow-based boundary element method software, ANSYS AQWA®, has been used, which provides first-order hydrodynamic excitation force, radiation added mass and damping, hydrostatic stiffness, and first- and second-order drift forces. Most importantly, thanks to a built-in package, mooring systems and environmental loads can be included in the mathematical model [23].

4.4.1. Pull-Out Tests

To assess the mooring static characteristics for both mooring configurations C1 and C2, the pull-out test was performed in calm water conditions. Starting from the equilibrium state of the WEC at the center of the three mooring lines, the device was pulled along the direction of one of the three mooring lines in order to obtain the restoring force in every step of 20 mm. The pull-out test continues until the mooring chain becomes totally stretched along the x-direction, as presented in Figure 10. The static forces induced by the moorings have been measured by the load cell, while the precise displacement of the body has been acquired by the QUALISYS® system. Two pull-out tests were performed, as shown in Table 5.

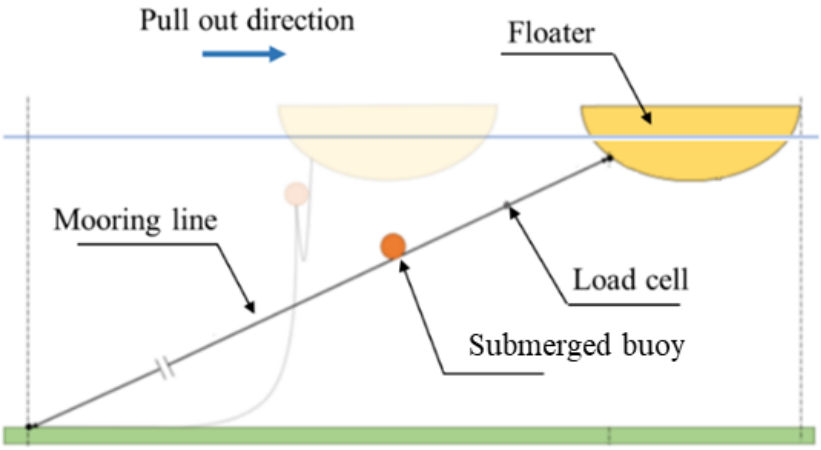

Figure 10. Pull-out test execution.

Table 5. Performed pull-out tests.

	Configuration		
ID	C1	C2a	C2b
Pull-out test	✓	✓	✗

Figure 11 shows the comparison between the numerical simulation in ANSYS AQWA® and the experimental results up-scaled to the prototype dimensions. The numerical results behavior shows an excellent agreement with the experimental one, with a relative error not exceeding 5%. Such an error percentage means that the numerical model is reliable for the calculation of the static characteristic and ensures a correct scaling according to the Froude scale. The load-excursion reported in Figure 11 is divided into two main parts: the first one reports an almost constant load behavior, while the second one shows that the load increases nonlinearly until the mooring line becomes taut.

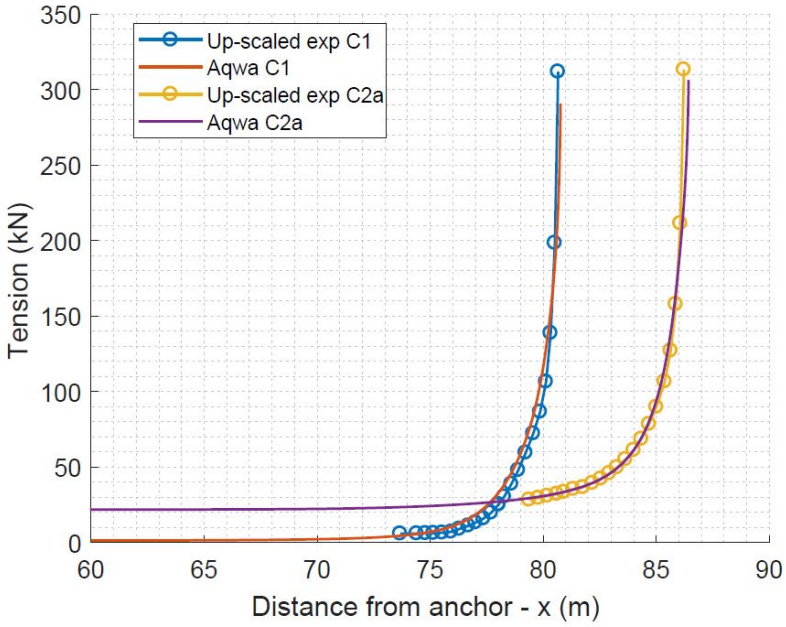

Figure 11. Static characteristics of the two mooring layouts.

4.4.2. Effect of Mooring on Pitch Natural Period and Damping

The pitch decay test has been performed with and without the mooring system, to confirm the expected small influence on the pitch natural period and damping levels. These tests have been performed in calm water, starting from 10deg, and the resulting decay curves are given in Figure 12. It can be noted that there is no significant effect of either mooring configuration on the pitch period and damping.

4.4.3. Regular Wave Tests

The monochromatic wave study has been carried out following the ITTC Recommended Procedures 7.5-02 -07-03.2 [44]. The prototype was tested in regular waves with a wave steepness of 1/50 for both mooring configurations and a wave steepness of 1/35 for configuration C1 only. The complete list of tests is provided in Table 6, including the wave ID, steepness (s), frequency (f), amplitude (A), and a checklist of the tests performed for the two mooring configurations. For the experimental tests, three wave probes were used: WP1 and WP3 positioned upstream of the device at the same longitudinal coordinate x, and WP2 positioned between the device and the tank wall.

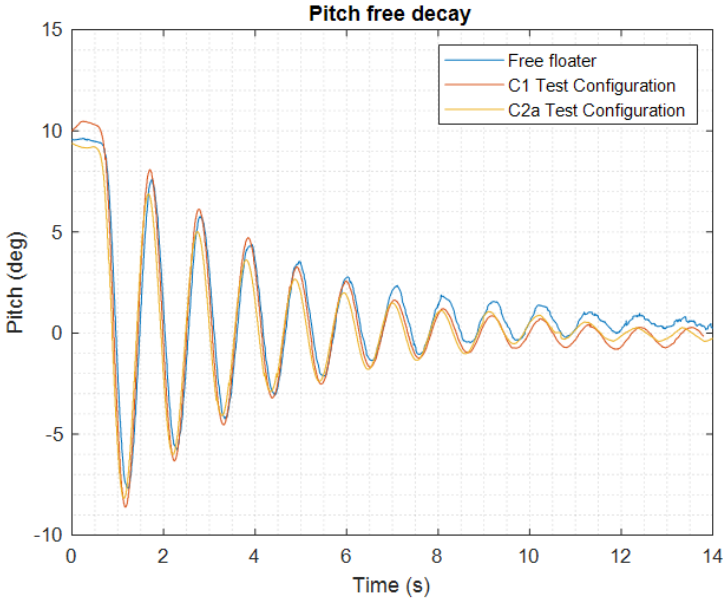

Figure 12. Pitch free decay experiments.

Table 6. Regular wave tests schedule.

Wave ID	s	f (Hz)	A (mm)	C1	C2a	C2b
1a	1/50	1.250	10.00	✓	✓	✗
2a	1/50	1.200	10.80	✓	✓	✗
3a	1/50	1.118	12.50	✓	✓	✗
4a	1/50	1.052	14.10	✓	✓	✗
5a	1/50	0.994	15.80	✓	✓	✗
6a	1/50	0.952	17.20	✓	✓	✗
7a	1/50	0.894	19.50	✓	✓	✗
8a	1/50	0.745	28.10	✓	✓	✗
9a	1/50	0.639	38.20	✓	✓	✗
10a	1/50	0.559	50.00	✓	✓	✗
11a	1/50	0.497	63.20	✓	✗	✗
12a	1/50	0.447	78.10	✓	✗	✗
3b	1/35	1.198	17.83	✓	✗	✗
5b	1/35	0.994	22.57	✓	✗	✗
6b	1/35	0.952	24.59	✓	✗	✗
7b	1/35	0.894	27.93	✓	✗	✗
9b	1/35	0.639	54.63	✓	✗	✗

4.4.4. Irregular Wave Tests

The irregular wave analysis has been performed according to the ITTC Recommended Procedures 7.5-02 -07-03.14 [45]. The irregular wave was described by the JONSWAP spectrum and the energetic period of the generated irregular wave was chosen to be close to the pitch resonant period of the floater, and therefore it is representative of the operational condition of the device. The characteristics of the tested irregular wave are provided in Table 7.

Table 7. Irregular wave tests schedule.

Wave ID	H_s	T_p (s)	γ	C1	C2a	C2b
Irr1	0.11	1.21	3.3	✓	✓	✗

4.4.5. Extreme Wave Tests

According to the DNV (Det Norske Veritas Group) procedures for positioning mooring [38], two different waves were considered to carry out the analyses of the mooring system in extreme wave conditions for the different mooring configurations: 100- and 10-year return period sea state for a three-hour storm. Concerning the 100-year return period wave, three wave records were tested, with each wave record characterized by the same spectral properties and different random phases (seeds) between the spectrum frequency components. Three seeds have been used to build a statistically relevant database for the mooring tensions analysis in extreme conditions. Furthermore, a 10-year return period sea state was tested. A single wave record was tested in these conditions to optimize the test schedule. Table 8 summarizes the tests carried out in extreme wave conditions.

Table 8. Extreme wave tests schedule.

Wave ID	H_s	T_p (s)	γ	Seed	C1	C2a	C2b
A10	0.250	1.950	3.3	1	✓	✓	✓
A101	0.295	2.303	3.3	1	✓	✓	✗
A102	0.295	2.303	3.3	2	✓	✓	✗
A103	0.295	2.303	3.3	3	✓	✓	✗

4.5. Uncertainty Analysis

Uncertainty analysis has been performed according to the ITTC (International Towing Tank Conference) Recommended Procedures 7.5-02-01-01 [46], based on the Type A and Type B uncertainty; for the towing tank at University Federico II, the detailed description of the uncertainty analysis can be found in [47]. Type B uncertainty for the wave probes is 0.3/1000 mm and repeatability 0.5/1000 mm. For the 95% confidence level, the total uncertainty is 1%. The Type B uncertainty related to measurement of model motions using an optical motion capture depends upon the setup of both cameras and markers and varies through the measurement volume. Typical values for the translation motions are 0.5/1000 mm, and up to 3% for the roll, pitch, and yaw motions.

5. Experimental Campaign Results

Three main outputs are analyzed: quantification of the hydrodynamic performances; operational mooring loads, and statistical distribution of mooring loads in extreme wave conditions.

5.1. Regular Wave Results

The six DoF device motions have been measured along with mooring loads and wave profiles. For each test, at least a 30 s interval where all motions that reached a steady response have been identified. In such intervals, the following quantities are analyzed in the time-domain as peak-to-peak: wave amplitude, heave and pitch motion amplitude, and force in the mooring line; in the frequency domain, results are computed by applying the Fast Fourier Transform (FFT) analysis.

The values of pitch and heave Response Amplitude Operator (RAO) were calculated to compare the performance of the floater considering the two mooring configurations. Moreover, comparison of the RAO obtained via numerical simulation and experimental testing can provide confidence in the model and a preliminary validation [48]. The RAO evaluation was performed according to the following equations:

$$RAO_3 = \eta_{30} / A, \tag{2a}$$

$$RAO_5 = \eta_{50}/kA, \tag{2b}$$

where η_{30} represents the heave motion amplitude, η_{50} the pitch motion amplitude, A the encounter wave amplitude, and k the wave number.

The experimental pitch and heave RAOs for both mooring configurations C1 and C2a, together with the numerical results obtained by ANSYS AQWA® with zero-forward speed and no-mooring conditions, are shown in Figures 13 and 14 as a function of the full scale wave period. For the sake of clarity, the experimental wave frequencies have been scaled to full scale in order to match the numerical simulations.

It can be seen that the introduction of the clump-mass in Configuration C2a has a slight influence on the motion amplitude. In average, the difference in pitch amplitude is up to 5% close to the resonance region. It can be noted that, at the resonant frequency, the difference between two points at different steepness is larger than the difference between different configurations. This is expected, due to the impact of nonlinearities. Since the objective of this part of experimental campaign was to investigate whether the efficiency of the WEC (in terms of pitch RAO) is affected by the mooring configuration C2, the measured differences within 5% only at the resonance have not been considered as penalizing. With regard to the comparison between numerical and experimental results, a general good agreement for pitch motion can be observed. It should be clarified that numerical RAOs are calculated for a free body and no mooring effects are included. The specific results are promising because it is demonstrated that the catenary mooring is suitable for operational conditions. Larger differences are found near resonance conditions with the highest difference of 15%. Such a disagreement can be justified by the basic hypothesis of the linear theory, namely the small amplitude waves and small amplitude motions that are severely challenged when the hull experiences large motions in resonance. Furthermore, in the resonance zone, the coupling effect between hull dynamics and mooring lines, which was neglected in the numerical simulations, is more significant.

The comparison of numerical and experimental results for heave RAO, presented in Figure 14, shows a good agreement for the steeper waves (steepness = 1/35), while the results in lower waves (steepness = 1/50) are over-predicted. It can be seen also that the heave response is lower when the clump-weight is included. However, heave motion does not contribute to the power conversion chain and lower response can be accepted for the sake of safety.

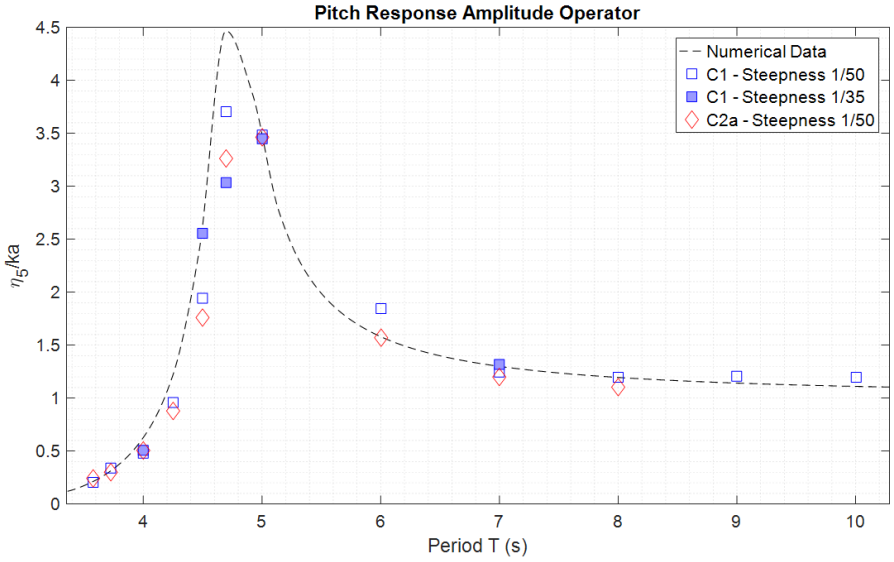

Figure 13. Experimental pitch RAOs compared with the free-floating pitch numerical RAOs.

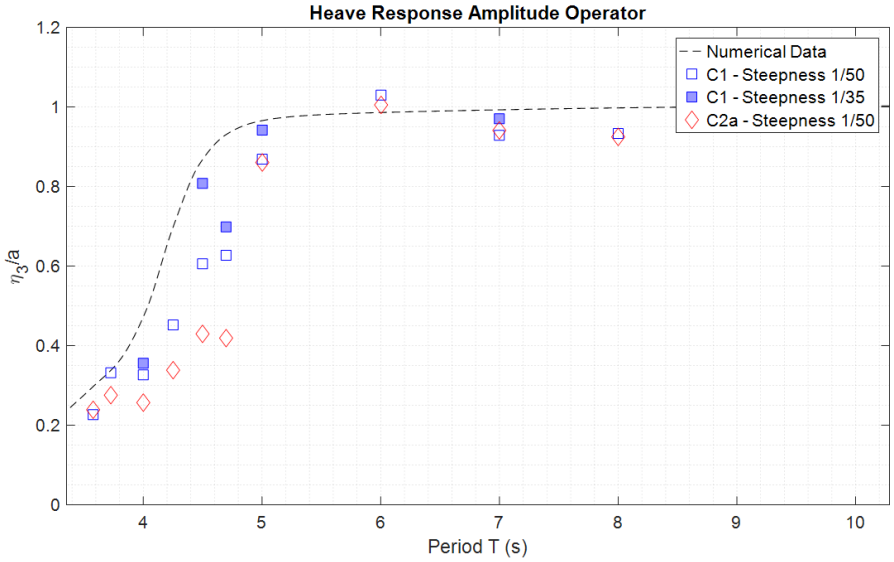

Figure 14. Experimental heave RAOs compared with the free-floating heave numerical RAOs.

5.2. Irregular Wave Results

Likewise, for the regular wave tests, the device motion along with the mooring load and wave profile has been measured and analyzed in irregular sea states in order to assess the mooring influence on the device performance in operating conditions.

5.2.1. Irregular Wave Spectral Analysis

For each irregular wave test, the spectral analysis has been performed on both the input signal of the wave generator and the measured waves. For this analysis, only wave probe 3 (WP3, see Figure 8) was considered, since ultrasonic wave gauges may lose the signal when there are high steepness waves or breaking waves.

Figure 15 reports the power spectral density (PSD) analysis of the wave profile signals, showing a good repeatability of the wave generator, since the measured wave spectra superimpose. Wave records analysis shows that the main spectral properties H_s and T_p are in good agreement with the desired ones, as reported in Table 9.

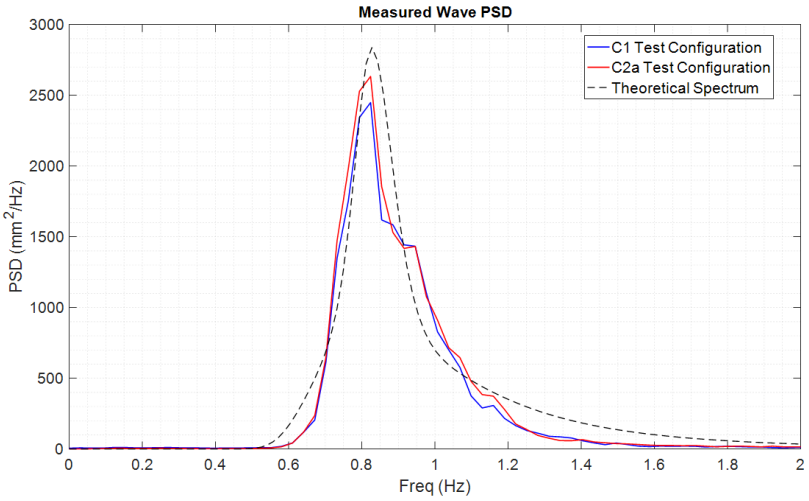

Figure 15. Measured irregular JONSWAP wave spectra compared with the theoretical spectrum.

Table 9. Irregular wave records spectral properties.

Wave ID	Configuration	H_s (m)	T_p (s)
Operational wave	Theoretical data	0.110	1.210
Irr1	C1	0.101	1.210
Irr1	C2a	0.104	1.210

5.2.2. Device Motion and Mooring Loads Analysis in Operational Wave Conditions

The influence of the two different mooring systems on the surge motion and the mooring loads is shown in Figure 16a,b, respectively.

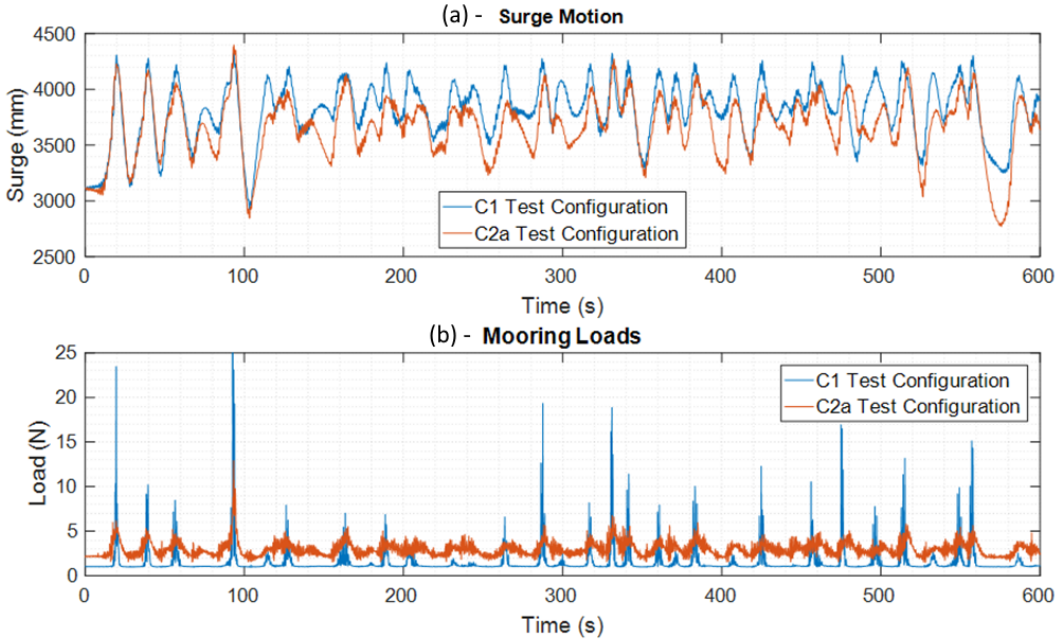

Figure 16. Surge (**a**) and mooring loads (**b**) time series for the two mooring configuration tests in the irregular wave condition.

The presence of the clump mass in mooring configuration C2a limits the surge motion and the mooring loads show an offset load higher than the case of configuration C1. On the other hand, mooring C2a highlights less snap peak loads, fundamental for the durability and survivability of the whole system. The weather-vane of the device is guaranteed by both mooring systems, as shown in Figure 17: both yaw and sway motions are restrained and therefore the property of the mooring layout to align the device with the incoming sea state is demonstrated.

The PSD (power spectral density) of heave motion, calculated from experimental data, for both mooring configuration C1 and C2a is shown in Figure 18, compared with the wave PSD (configuration C2a test case).

In accordance with the heave RAO, shown in Figure 14, at low frequencies, the heave PSD follows the wave PSD and shows higher amplitude attenuation towards higher frequencies.

The measured pitch motion for both mooring configurations is shown in Figure 19.

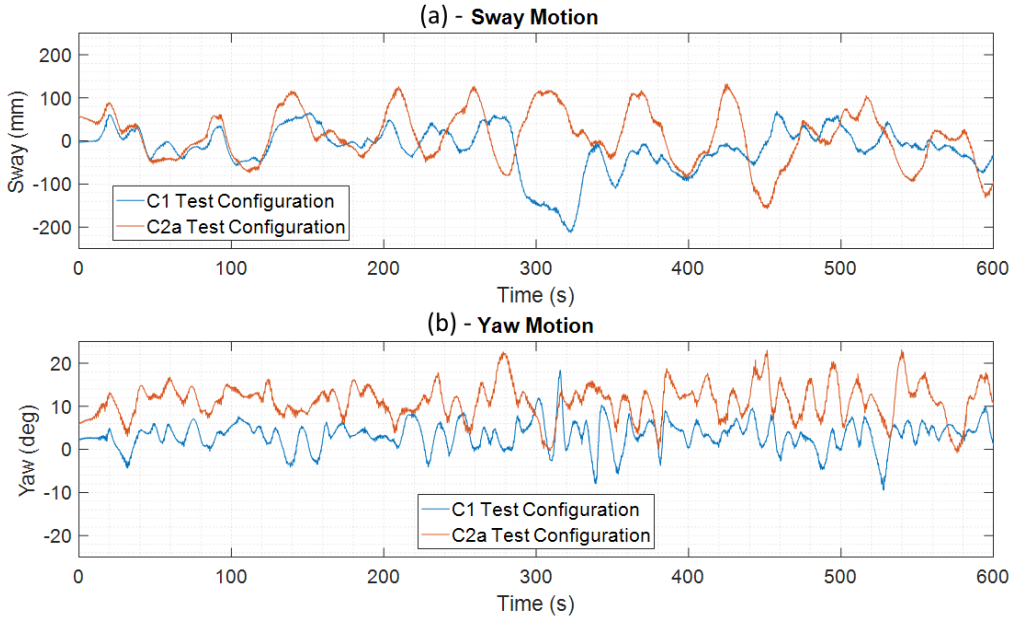

Figure 17. Sway (**a**) and yaw (**b**) time histories for the two mooring configuration tests in the irregular wave condition.

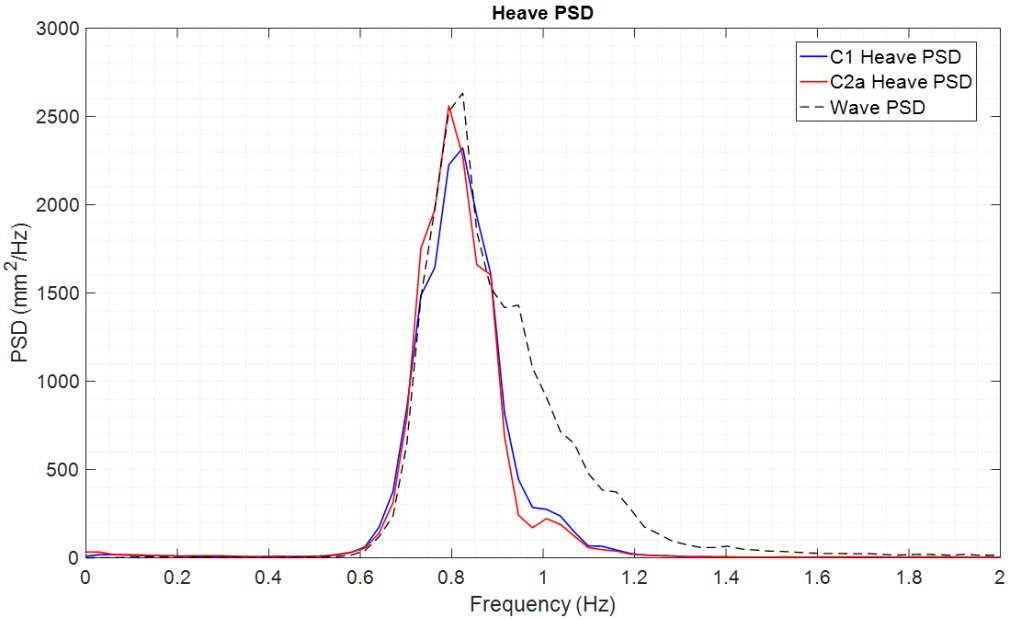

Figure 18. PSD of the heave motion and incoming wave.

As expected from the free decay and regular wave analysis, the pitch PSD peak is close to its damped natural period, and no significant differences between the two mooring configurations are obtained. Therefore, the presence of the clump-weight and the higher stiffness of mooring configuration C2a does not compromise the performance of the device in operational conditions. The RMS values of the heave (z_{RMS}), roll (α_{RMS}), and pitch (δ_{RMS}) motions are shown in Table 10 and have been calculated as follows:

$$\eta_{i_{RMS}} = \int_{f_i}^{f_{end}} PSD_{\eta_i}(f)\ df \tag{3}$$

where $\eta_{i_{RMS}}$ is the Root Mean Square (RMS) value of the i-DoF, f is the frequency, and PSD_{η_i} is the Power Spectral Density of the i-DoF. The RMS pitch motion in the presence of C2a mooring layout shows a decrease of 2.3% in operational sea state condition as shown in Table 10. This performance decrease of performance is acceptable in view of the higher mooring stiffness and a reduction of mooring peak loads. Moreover, the roll motion for both mooring configurations is restrained and thus the floater stability in roll is demonstrated.

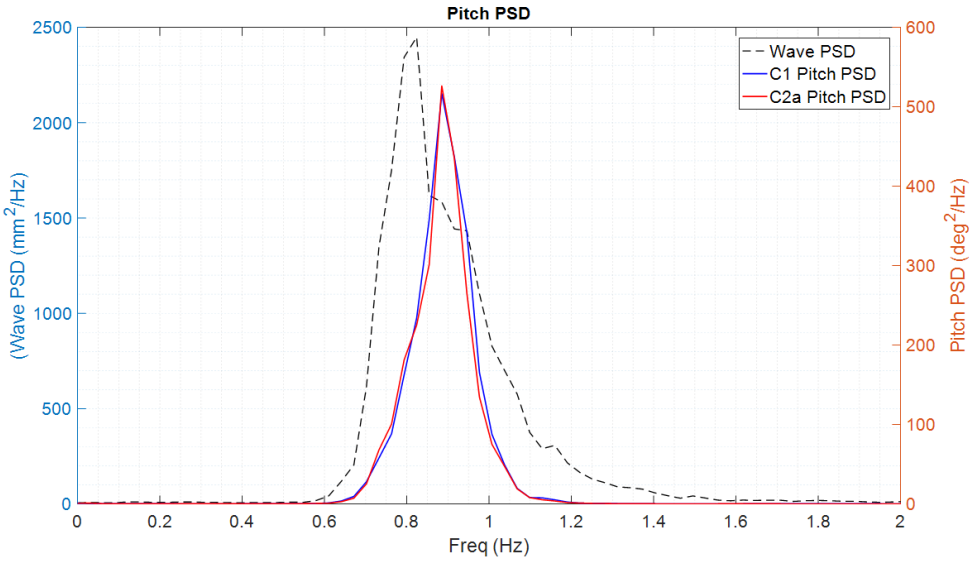

Figure 19. PSD of the pitch motion.

Table 10. RMS values of the floater motion in irregular wave.

Wave ID	Configuration	δ_{RMS} (deg)	z_{RMS} (m)	α_{RMS} (deg)
Irr1	C1	8.83	0.22	1.11
Irr1	C2a	8.63	0.22	1.44

5.3. Extreme Waves Analysis

Configurations C1 and C2a have been tested in secular sea states, respectively without and with the clump-weight on the mooring lines. On the 10-year return period wave, the attention was focused on the load reduction. In particular, a further modification of the mooring system was tested: a bigger clump-weight was introduced to investigate the influence of the mass on the tension peaks (Configuration C2b). In fact, as demonstrated in this section, the effect of the clump-weight is decisive for the reduction of snaps and loads. Six sea-keeping tests were performed for the 100-year return period sea states, and three sea-keeping tests for the 10-year return period wave.

5.3.1. Extreme Waves Spectral Analysis

As far as the spectral analysis of the extreme sea states time records is concerned, the same procedure of the irregular waves has been considered. Figure 20 reports the spectral analysis for the wave profile signals of the 100-year return period incident wave tests. Again, this figure demonstrates a very good repeatability of the wave generator, the measured wave spectra being superimposed. To avoid redundancy of information, only the 100-year wave spectrum with the mooring configuration C2a wave has been reported.

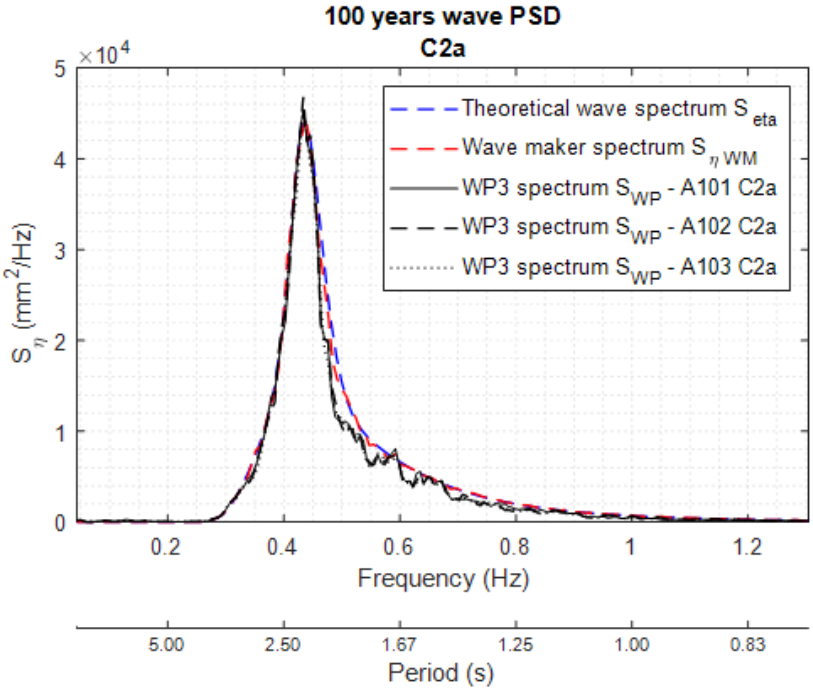

Figure 20. Waves power spectral density: 100-year wave.

Table 11 shows the results summary for all tested waves. In short, wave records analysis shows that the main spectral properties H_s and T_p are in good agreement with the target ones.

Table 11. Extreme wave records spectral properties.

Wave ID	Configuration	H_s (m)	T_p (s)
10-year wave	Theoretical data	0.250	1.950
A10	C1	0.251	1.950
A10	C2a	0.253	1.950
A10	C2b	0.253	1.950
100-year wave	Theoretical data	0.295	2.303
A101	C1	0.276	2.308
A102	C1	0.286	2.307
A103	C1	0.294	2.307
A101	C2a	0.295	2.308
A102	C2a	0.294	2.310
A103	C2a	0.292	2.306

5.3.2. Device Motion Analysis in Extreme Wave Conditions

A proper evaluation of the hydrodynamic behavior in extreme wave conditions of the floating body is crucial for both design stage and operational analyses of the survivability of a WEC. As for the wave profiles analysis, analogous results were found for both 100- and 10-year waves conditions. To avoid repetitions, 10-year wave results are presented and commented on in detail here.

Firstly, the heave motion is analyzed and compared with the incident wave. Figure 21 reports the heave power spectral density for the configurations C1 and C2a, respectively, in Figure 21a,b. It is possible to observe that the heave response is not influenced by the mooring system modifications. The peak of the motion response coincides with the wave frequency: this means that there is no slow-frequency contribution in heave.

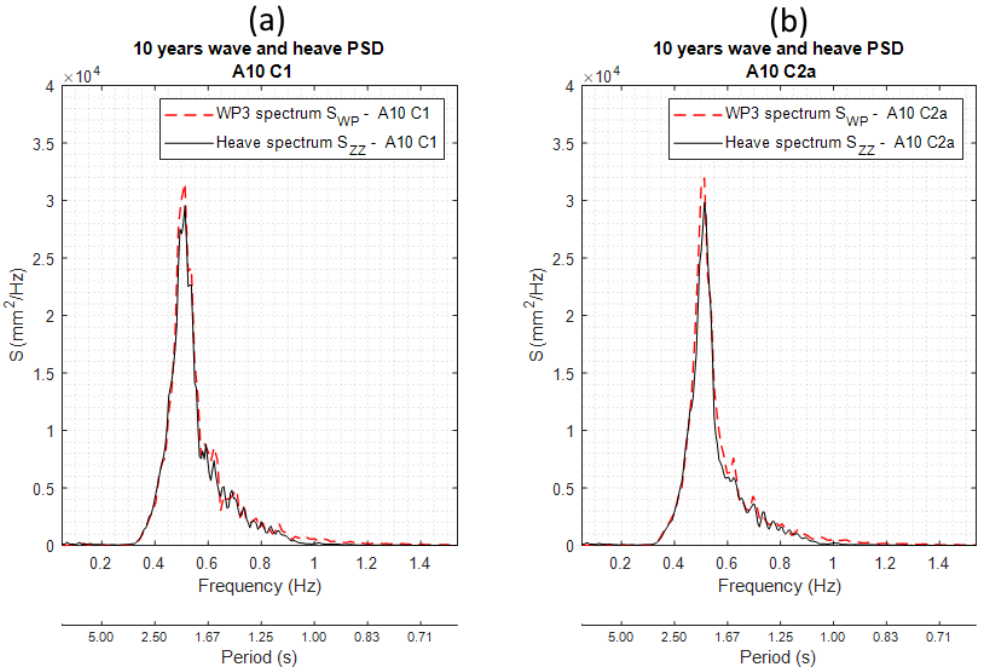

Figure 21. Heave motion spectral density for C1 (**a**) and C2a (**b**) 10-year wave.

The surge motion is the most important from the mooring design point of view. From Figure 22, it is possible to observe that the energy contribution to the surge motion is mainly distributed at a very low frequency. For surge motion, the second order wave forces are mainly important, since they excite the mooring system natural frequency (see Figure 22b). Moreover, a zoom is needed to investigate the second peak of the surge PSD (see Figure 22c). This peak corresponds to the first order forces contribution of the incident wave: it is immediate to notice that this area of the surge PSD follows the wave power spectrum, but its power content is two orders of magnitude below the low frequency area.

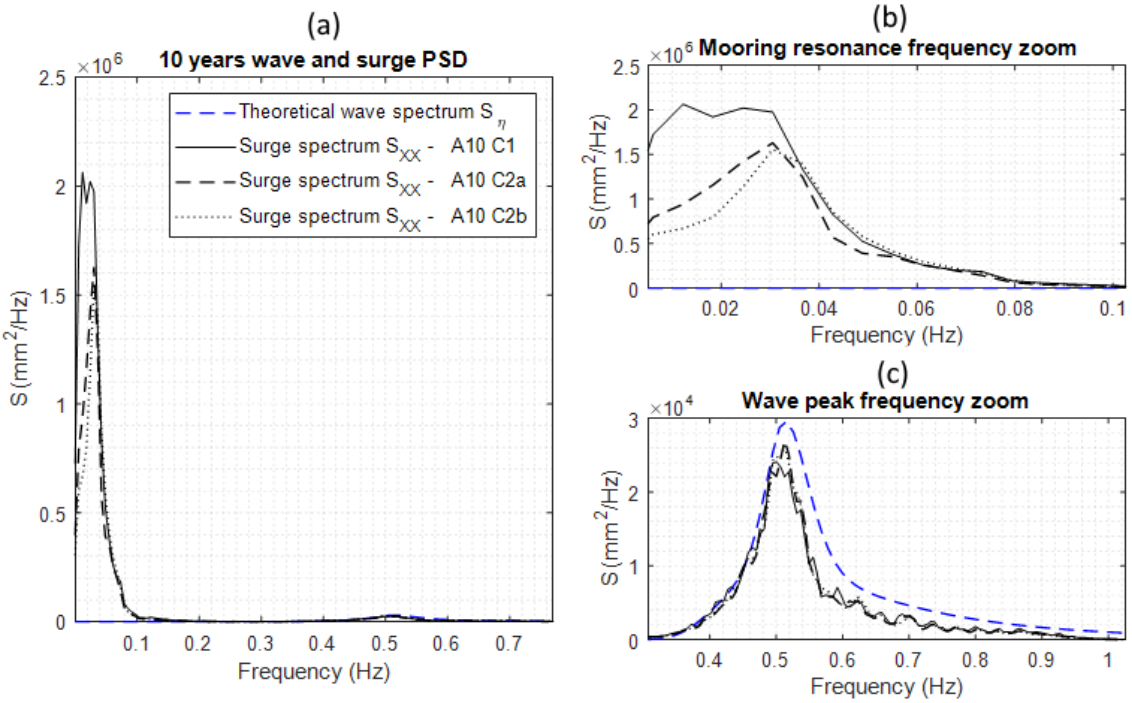

Figure 22. Surge motion and wave spectral density in (**a**), with zooms in (**b**) at the mooring resonance frequency, and in (**c**) around the wave peak frequency: 10-year wave.

This result demonstrates that the first order forces contribution to the surge motion can be neglected with a good approximation. Furthermore, the mooring systems' natural frequencies can be identified by evaluating the peak frequency of the power spectrum for each configuration. Introducing the clump-weight, the stiffness of the moored system in surge increases, thus reducing the natural period. Consequently, the motion of the device is restrained, and the surge displacement results are lower on average. This is confirmed by the summary reported in Table 12: specifically, a reduction of both RMS value (x_{RMS}) of the surge motion and its peak period (T_{px}) is observed increasing the clump weight.

Table 12. Surge motion spectral properties: 10-year wave.

Wave ID	Configuration	x_{RMS} (m)	T_{px} (s)
A10	C1	3.050	82
A10	C2a	2.570	34
A10	C2b	2.460	32

Regarding the pitch motion, Figure 23 relates the pitch motion response to the incident wave. Focusing on the black lines, which refer to the pitch PSDs of the device, they are similar for each test and exhibit two peaks. The lower frequency peak corresponds to the peak period of the incident wave, equal to 1.95 s, while the higher frequency one corresponds to the damped natural pitch period of the device, equal to 1.07 s. It is interesting to highlight that the pitch PSD peak is close to the device damped period and no big differences between the three mooring configurations are shown, as found in the irregular wave tests. This means that, despite the wave energy contribution being relatively low around 1.07 s, the pitch motion is still amplified due to the inertia properties of the hull. The motion of the device is governed by its inertia properties.

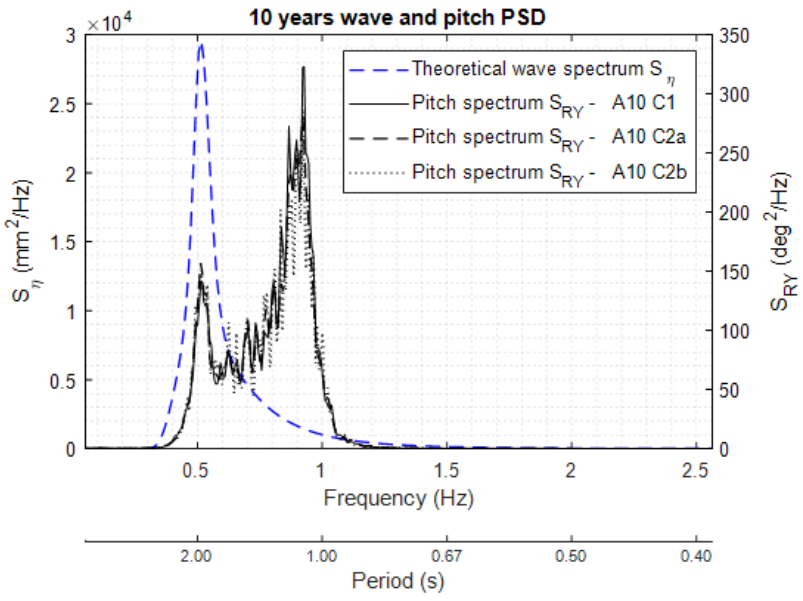

Figure 23. Pitch motion spectral density: 10-year wave.

Regarding the heave and surge motion, Table 13 reports a summary of the main results of the pitching motion, highlighting that pitch is also not influenced by the mooring system in extreme wave conditions (the RMS value δ_{RMS} and the peak period $T_{\delta p}$ of the pitching motion are not affected by the clump-weight).

Table 13. Pitch motion spectral properties: 10-year wave.

Wave ID	Configuration	δ_{RMS} (deg)	$T_{\delta p}$ (s)
A10	C1	8.30	1.078
A10	C2a	8.23	1.085
A10	C2b	8.09	1.085

From the motion spectral analysis, it is not possible to evaluate which mooring system has the best performances. More precisely, all the tested configurations demonstrated good performances in terms of the influence on the dynamics of the floater for high power sea states. On the other hand, the critical design point in extreme wave condition is the evaluation of the survivability of the mooring system in terms of mechanical failures.

5.3.3. Mooring Loads Analysis in Extreme Wave Conditions

To quantify the loads and their statistical distribution for each mooring configuration, the signal of a load cell installed just after the swivel was acquired. Figure 24 shows a time trace window of the mooring load signal (Figure 24a), compared against the wave free surface elevation (Figure 24b), surge (Figure 24c), and pitch signal (Figure 24d), for Configuration C2a and the 10-year wave test. It is worth remarking that the pitch dynamics is governed by the damped natural frequency of the device. Furthermore, the surge motion also presents a lower frequency contribution due to the natural frequency of the mooring system. From the third subplot, it is possible to confirm that the low frequency excites the mooring lines. Mooring loads are characterized by a very low mean load, which is mainly due to the catenary weight, and singular spikes of higher orders of magnitude.

The extreme event occurs when high amplitude displacements are recorded in the same instants for surge and pitch motions. The high amplitude displacements are a consequence of the drift loads due to the wave group that precedes the extreme event (noted by two vertical dashed lines in the second subplot). Unfortunately, it has not been possible to find a relation between the properties of the wave group and the occurrence of the extreme event. More precisely, it can be observed that the wave group does not look different from other windows of the time-series sample. Nevertheless, the correspondence of high amplitude displacement is observed only once. This is due to the combination of several factors that cannot be controlled or separated in the dynamic evolution of the system. The adverse combination of these motions leads to the full extension of the mooring lines. When the line reaches its maximum extension, the chain is completely lifted from the seabed and a snatch load occurs. Snaps are governed by the device drift and they can be identified as isolated events during the storm. To analyze such events, neither a time domain nor a spectral analysis is appropriate. Hence, a statistical approach is proposed here.

The statistical analysis is performed for the 100- and 10-year return period waves tests. The three tested configurations (C1, C2a, and C2b) are analyzed in order to identify the best solution for the ISWEC mooring system. Table 14 tabulates the RMS value and maximum peak of tension for each test in extreme waves. From these results, it is possible to observe a clear improvement from configuration C1 to configuration C2a and then to Configuration C2b in terms of tension peaks' reduction. In more detail, considering the 10-year wave, a reduction of the maximal peak value of almost 48% can be observed by employing the Configuration C2a instead of the Configuration C1. Moreover, by employing the Configurations C2b, a reduction of almost 60% can be reached. Analogous results were found for the 100-year wave: a considerable reduction of the maximal peak value of the mooring load can be obtained with the introduction of the clump weight. The same behavior is observed with different seeds: this means that there is no evident influence of the random phase between frequency components on different mooring configurations. Finally, note that, due to limited time available for experimental testing in the wave tank, configuration C2b was tested only for the 10-year wave.

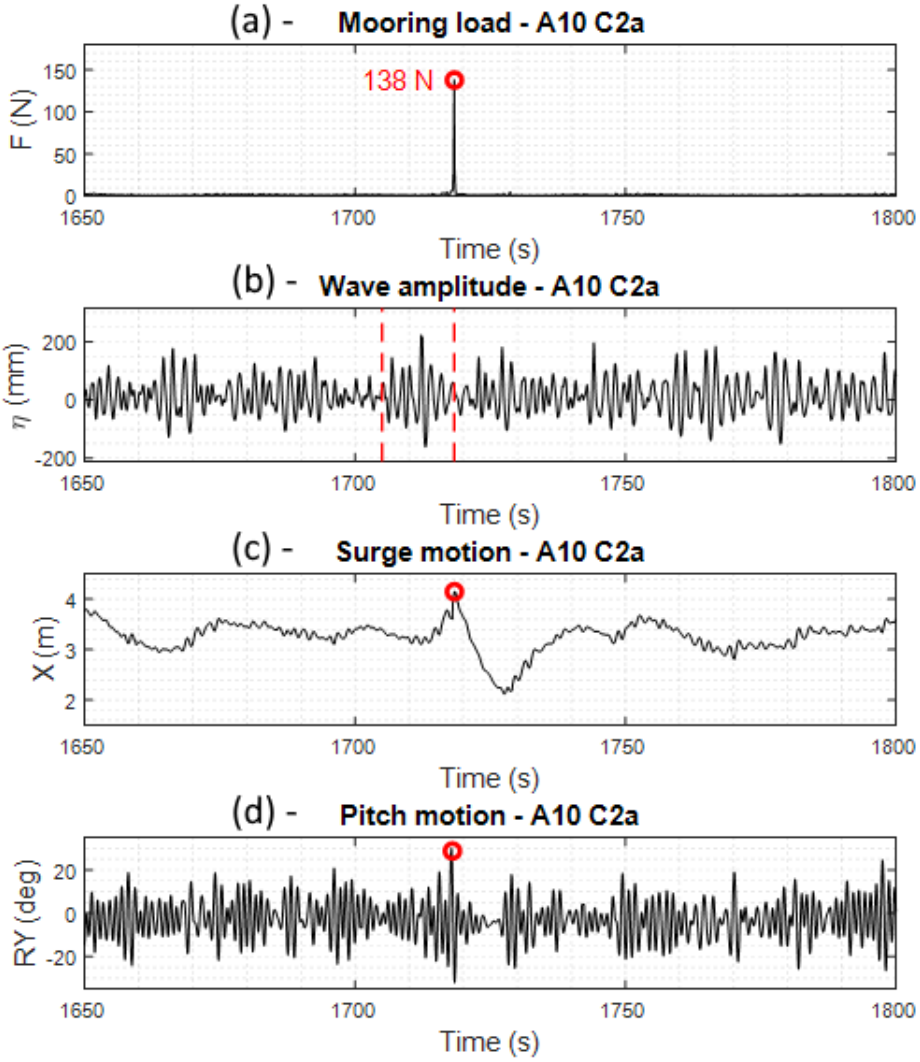

Figure 24. Time traces sample: 10-year wave, Configuration C2a.

Table 14. Root mean square value and maxima peaks of mooring tension: 10- and 100-year waves.

Wave ID	Configuration	F_{RMS} (N)	F_{max} (N)
A10	C1	3.4	264
A10	C2a	2.0	138
A10	C2b	1.7	107
A101	C1	2.7	186
A102	C1	3.1	210
A103	C1	3.2	405
A101	C2a	2.3	19
A102	C2a	1.7	23
A103	C2a	2.3	61

Moreover, Table 14 shows that both the maxima of the extreme events and the RMS are comparable for 10-year and 100-year waves. This means that the worst load case is not necessarily correlated to the power content of the wave. Furthermore, Table 14 gives an indication on the order of magnitude of the maximum expected tension for the full-scale mooring system. On the other hand, the maxima show relevant differences among the tests with the same mooring configuration. Assuming that the

number of peaks per each configuration represents a statistically relevant sample, it is interesting to investigate the probability distribution of the peaks. In Figure 25, the peak distribution is shown for Configurations C1 and C2a in a secular wave. In fact, the 100-year return period extreme wave condition is the wave that dictates design requirements.

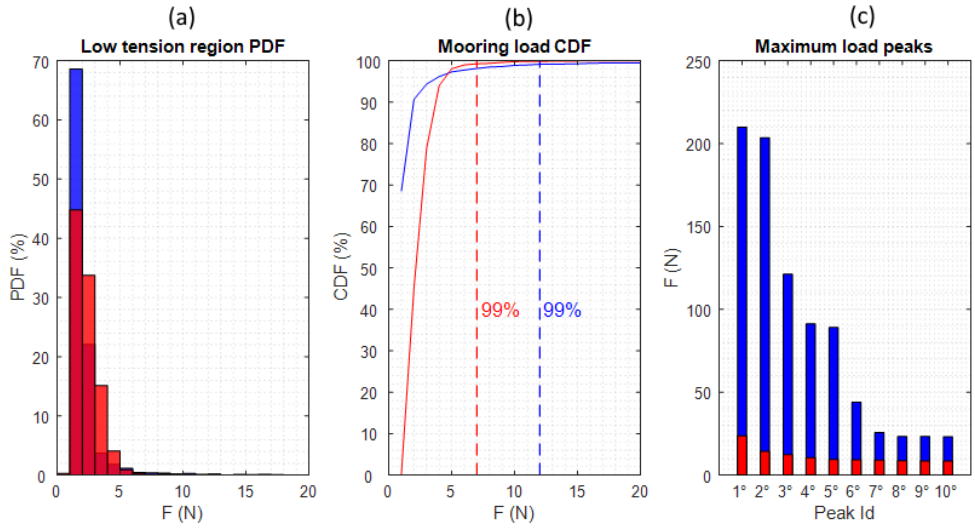

Figure 25. Mooring loads statistical distribution (PDF: probability density function; CDF: cumulative density function): 100-year wave, C1 (in blue:) and C2a (in red:) configurations.

The chart in Figure 25a reports the Probability Density Function (PDF) of the load peaks. It is clear that the majority of the peaks are distributed in the low-tension region, for both configurations. Indeed, the zoomed region corresponds to the 99% of the detected peaks. Below this threshold, it can be assumed, with a good fidelity, that the mooring loads are representative of the normal working conditions. Above the threshold, the peaks can be considered as extreme isolated events. As shown by the Cumulative Density Function (CDF), 99% of the detected peaks are significantly lower than the maximum load peaks. Comparing the two mooring configurations, the experimental PDF has the same shape for both configurations, but, in Configuration C2a, the tension's peaks are considerably lower. In particular, the ten highest peaks of the mooring load are lower in the C2a configuration. For the sake of clarity, the ten highest peaks of the mooring load are the ten highest values of the mooring load referred to a single extreme wave test for the configurations considered. The same analysis is performed for three tests in 10-year waves with different mooring configurations.

Focusing on the mooring load time traces (see Figure 26), it can be noticed that the extreme peaks can be reduced by employing the clump-weight configuration. For a better visualization, the tension values are reported on a logarithmic scale and four extreme events are highlighted with markers. In more detail, considering the four highest peaks of the time window, a reduction of the load peaks from 59% up to 96% can be achieved with the clump-weight configurations with respect to the Configuration C1.

Moreover, it is observed that the extreme events occur exactly at the same instant for all the tests. Hence, it is clear that these events are related to a specific combination of motion and loads. On the other hand, it is not possible to identify a univocal relation between the mooring properties and the peak values.

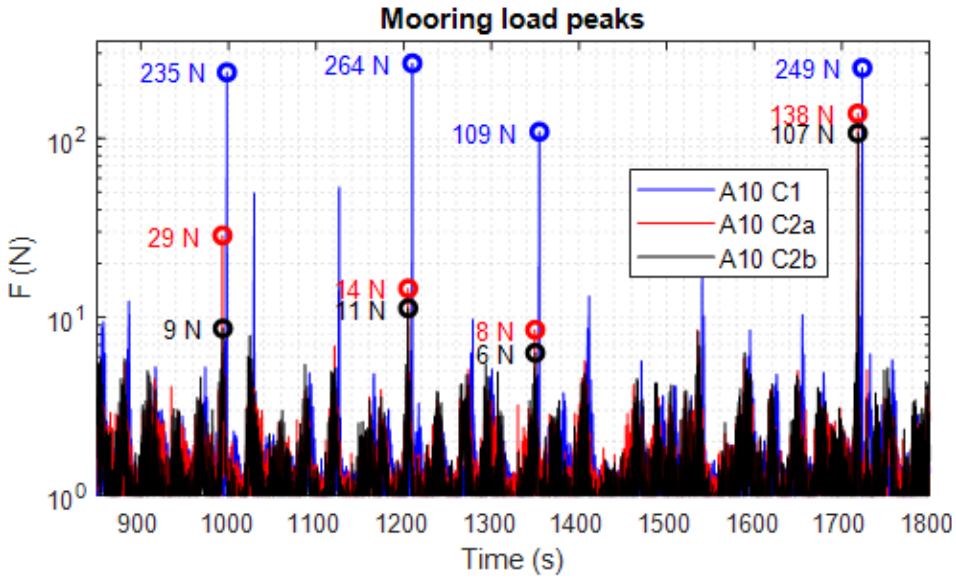

Figure 26. Mooring load time traces sample: 10-year wave, C1, C2a, and C2b configurations.

6. Conclusions

The results of the experimental campaign on the mooring system of the 1:20 ISWEC scaled model carried out in the towing tank of University of Naples Federico II have been presented and discussed. The mooring system design here presented is based on the Pantelleria installation site because it is a known site from the point of view of Meteocean data, and it is significantly severe from the point of view of extreme wave conditions. The proposed mooring configuration assures the good station keeping of the floater during operation and allows the device to align itself with the dominant sea state direction. The choice and design of the mooring system is a trade-off among energy extraction performances, survivability capabilities, and load reduction. The influence of adding a clump weight in the mooring lines on the floater dynamics and mooring loads is studied.

Firstly, it has been demonstrated that the experimental static characteristics of two mooring configurations agree well with the numerical simulations, and it was shown that mooring C2a has a higher capacity of energy absorption than C1 but acts with higher static mooring loads on the hull. The insertion of the clump-weights in the mooring lines does not compromise the amplitude of the pitch oscillation of the floater in regular waves. Consequently, in regular waves, the performances of the device in terms of extracted energy are comparable for both mooring layouts.

The 1:20 ISWEC model was tested in regular and irregular waves to study the performance of the system in operational conditions. As expected from the regular wave analysis, no relevant differences on pitch motion were revealed between the two mooring systems. Moreover, the ISWEC model was aligned with the incoming wave during the whole test, demonstrating the capability of the mooring layouts to weathervane. It has been possible to demonstrate how the addition of the clump-weight influences the natural period of the mooring system: the clump-weight determines an increase of the stiffness of the system and a consequent decrease of the natural period. Furthermore, this effect is demonstrated by the reduction of the RMS values of surge motion with increasing clump-weight mass.

For what concerns the load of the mooring system, a time domain and a statistical analysis have been performed in extreme sea states' conditions. Firstly, four time traces have been presented, concerning the mooring load, wave elevation, surge motion, and pitch motion for Configuration C2a and the 10-year wave. It was assessed that the pitch motion is governed by the damped natural frequency of the device and the surge motion from the mooring natural frequency. Mooring loads are characterized by a low mean load, mainly due to the catenary weight, and singular spikes of higher orders of magnitude than the mean. Such extreme events occur when the mooring line reaches its maximum extension, and the chain is completely lifted from the seabed. Unfortunately, it has not been

possible to find a correlation between the properties of the wave group, the device's motion, and the occurrence of the extreme event. More precise considerations regarding load peaks can be given by the statistical approach proposed here. From the results, it is possible to demonstrate that the insertion of a clump-weight on the mooring line is a relevant improvement in the design, allowing a relevant reduction of the mooring loads. A relevant reduction of maximal peak values can be observed, from almost 48% up to 96% by employing the clump-weight solution. Moreover, the majority of the peaks are distributed in the low-tension region for both configurations. The low-tension region represents 99% of the detected peaks and therefore it can be assumed with a good fidelity that these loads are representative of the normal working conditions.

Author Contributions: Conceptualization, S.A.S., M.B., E.B., C.B., P.D., G.B., and G.M.; methodology, S.A.S., M.B., E.B., C.B., P.D., G.B., and G.M.; software, S.A.S., M.B., and P.D.; validation, S.A.S., M.B., and P.D.; formal analysis, S.A.S., M.B., E.B., C.B., P.D., G.B., and G.M.; investigation, S.A.S., M.B., and P.D.; resources, S.A.S., M.B., E.B., C.B., P.D., G.B., and G.M.; data curation, S.A.S., M.B., E.B., C.B., P.D., G.B., and G.M.; writing—original draft preparation, S.A.S., M.B., and G.G.; writing—review and editing, S.A.S., M.B., and G.G.; visualization, S.A.S., M.B., and G.G.; supervision, G.B., and G.M.; project administration, G.B. and G.M.; funding acquisition, G.B. and G.M. All authors have read and agreed to the published version of the manuscript.

Funding: This research has partially received funding from the European Research Executive Agency (REA) under the European Union's Horizon 2020 research and innovation program under Grant No. 832140.

Conflicts of I nterest: The authors declare no conflict of in terest. The funders had no role in the design of the study; in the collection, analyses, or interpretation of data; in the writing of the manuscript, or in the decision to publish the results.

References

1. Barltrop, N. *Floating Structures: A Guide for Design and Analysis*; Oilfield Pubns Inc.: Houston, TX, USA, 1998.
2. Paredes, G.M.; Bergdahl, L.; Palm, J.; Eskilsson, C.; Pinto, F.T. Station keeping design for floating wave energy devices compared to floating offshore oil and gas platforms. In Proceedings of the 10th European Wave and Tidal Energy Conference, Aalborg, Denmark, 2–5 September 2013.
3. Giorgi, G.; Ringwood, J.V. Articulating parametric resonance for an OWC spar buoy in regular and irregular waves. *J. Ocean Eng. Mar. Energy* **2018**, *4*, 311–322. [CrossRef]
4. Gao, Z.; Bingham, H.B.; Ingram, D.; Kolios, A.; Karmakar, D.; Utsunomiya, T.; Catipovic, I.; Colicchio, G.; Miguel Rodrigues, J.; Adam, F.; et al. *Committee V.4 Report: Offshore Renewable Energy, Vol. II*; Kamisnski, M.L., Rigo, P., Eds.; International Ship Offshore Structures Congress Press: Amsterdam, The Netherlands, 2018; pp. 193–277. [CrossRef]
5. Giorgi, G.; Ringwood, J.V. Analytical Formulation of Nonlinear Froude-Krylov Forces for Surging-Heaving-Pitching Point Absorbers. In Proceedings of the ASME 2018 37th International Conference on Ocean, Offshore and Arctic Engineering, Madrid, Spain, 17–22 June 2018.
6. Goggins, J.; Finnegan, W. Shape optimisation of floating wave energy converters for a specified wave energy spectrum. *Renew. Energy* **2014**, *71*, 208–220. [CrossRef]
7. Thomsen, J.B.; Ferri, F.; Kofoed, J.P. Assessment of Current State of Mooring Design in the Danish Wave Energy Sector. In Proceedings of the 11th European Wave and Tidal Energy Conference, Nantes, France, 6–11 September 2015; number 2015 in European Wave and Tidal Energy Conference Series.
8. Giorgi, G.; Gomes, R.P.F.; Bracco, G.; Mattiazzo, G. The Effect of Mooring Line Parameters in Inducing Parametric Resonance on the Spar-Buoy Oscillating Water Column Wave Energy Converter. *J. Mar. Sci. Eng.* **2020**, *8*, 29. [CrossRef]
9. Sheng, W.; Lewis, T.; Alcorn, R.; Johaning, L.; Kirrane, P. Experimental Investigation of Hydrodynamic Characteristics of a Moored Floating WEC. In Proceedings of the 3rd International Conference on Ocean Energy, Bilbao, Spain, 6–8 October 2010; pp. 1–9.
10. Hann, M.; Greaves, D.; Raby, A. Snatch loading of a single taut moored floating wave energy converter due to focussed wave groups. *Ocean Eng.* **2015**, *96*, 258–271. [CrossRef]
11. Paredes, G.M.; Palm, J.; Eskilsson, C.; Bergdahl, L.; Taveira-Pinto, F. Experimental investigation of mooring configurations for wave energy converters. *Int. J. Mar. Energy* **2016**, *15*, 56–67. [CrossRef]

12. Wu, M.; Stratigaki, V.; Verbrugghe, T.; Troch, P.; Altomare, C.; Crespo, A.; Kisacik, D.; Cappietti, L.; Dominguez, J.; Hall, M.; et al. Experimental study of motion and mooring behavior of a floating oscillating water column wave energy converter. In Proceedings of the 7th International Conference on Physical Modelling in Coastal Science and Engineering (Coastlab'18), Santander, Spain, 22–26 May 2018; pp. 1–8.
13. Sirigu, S.A.; Bracco, G.; Bonfanti, M.; Dafnakis, P.; Mattiazzo, G. On-board sea state estimation method validation based on measured floater motion. *IFAC-PapersOnLine* **2018**, *51*, 68–73. [CrossRef]
14. Tarrant, K.R.; Meskell, C. Investigation on parametrically excited motions of point absorbers in regular waves. *Ocean Eng.* **2016**, *111*, 67–81. [CrossRef]
15. Clément, A.H.; Babarit, A.; Gilloteaux, J.C.; Josset, C.; Duclos, G. The SEAREV wave energy converter. In Proceedings of the 6th Wave and Tidal Energy Conference, Glasgow, UK, 29 August–2 September 2005.
16. Wello, O. website 2020. Available online: www.wello.eu (accessed on 1 January 2020).
17. Falcão, A.F. Wave energy utilization: A review of the technologies. *Renew. Sustain. Energy Rev.* **2010**, *14*, 899–918. [CrossRef]
18. Aderinto, T.; Li, H. Ocean Wave energy converters: Status and challenges. *Energies* **2018**, *11*, 1250. [CrossRef]
19. Sheng, W. Wave energy conversion and hydrodynamics modeling technologies: A review. *Renew. Sustain. Energy Rev.* **2019**, *109*, 482–498. [CrossRef]
20. Karimirad, M.; Koushan, K.; Weller, S.; Hardwick, J.; Johanning, L. Applicability of offshore mooring and foundation technologies for marine renewable energy (MRE) device arrays. In *Renewable Energies Offshore*; Guedes Soares, C., Ed.; CRC Press: Boca Raton, FL, USA, 2015; pp. 905–912.
21. Ricci, P.; Rico, A.; Boscolo, F.; Villate, J.L. Design, Modelling and Analysis of an Integrated Mooring System for Wave Energy Arrays. In Proceedings of the 4th International Conference on Ocean Energy, Dublin, Ireland, 17–19 October 2012; pp. 1–6.
22. Bracco, G.; Cagninei, A.; Casassa, M.; Giorcelli, E.; Giorgi, G.; Mattiazzo, G.; Passione, B.; Poggi, D.; Raffero, M.; Vissio, G. Modeling and optimization of a Wave Energy Converter using ANSYS AQWA. In *Innovabook 2015. Paper Anthology. Fluidodinamica, Meccanica, Elettromagnetismo*; ANSYS User Group Meeting 2014; Cobalto Casa Editrice: Bergamo, Italy, 2015; pp. 79–86.
23. Davidson, J.; Ringwood, J.V. Mathematical modeling of mooring systems for wave energy converters—A review. *Energies* **2017**, *10*, 666. [CrossRef]
24. Harris, R.E.; Johanning, L.; Wolfram, J.; Frsa, M. Mooring systems for wave energy converters: A review of design issues and choices. In Proceedings of the 3rd International Conference on Marine Renewable Energy, Blyth, UK, 7–9 July 2004; pp. 159–168.
25. Martinelli, L.; Ruol, P.; Cortellazzo, G. On mooring design of wave energy converters: The seabreath application. In Proceedings of the Coastal Engineering Conference, Santander, Spain, 1–6 July 2012; pp. 1–12. [CrossRef]
26. Zanuttigh, B.; Martinelli, L.; Castagnetti, M. *Screening of Suitable Mooring Systems*; Technical Report; Aalborg University: Aalborg, Denmark, 2011; doi:10.13140/RG.2.1.1386.7048. [CrossRef]
27. Cagninei, A.; Raffero, M.; Bracco, G.; Giorcelli, E.; Mattiazzo, G.; Poggi, D. Productivity analysis of the full scale inertial sea wave energy converter prototype: A test case in Pantelleria Island. *J. Renew. Sustain. Energy* **2015**, *7*, 061703. [CrossRef]
28. Bracco, G.; Casassa, M.; Giorcelli, E.; Giorgi, G.; Martini, M.; Mattiazzo, G.; Passione, B.; Raffero, M.; Vissio, G. Application of sub-optimal control techniques to a gyroscopic Wave Energy Converter. *Renew. Energ. Offshore* **2014**, *1*, 265–269.
29. Bracco, G.; Giorcelli, E.; Mattiazzo, G.; Orlando, V.; Raffero, M. Hardware-In-the-Loop test rig for the ISWEC wave energy system. *Mechatronics* **2015**, *25*, 11–17. [CrossRef]
30. Bracco, G.; Giorcelli, E.; Giorgi, G.; Mattiazzo, G.; Passione, B.; Raffero, M.; Vissio, G. Performance assessment of the full scale ISWEC system. In Proceedings of the 2015 IEEE International Conference on Industrial Technology (ICIT), Seville, Spain, 17–19 March 2015; pp. 2499–2505. [CrossRef]
31. Sirigu, S.A.; Bonfanti, M.; Passione, B.; Begovic, E.; Bertorello, C.; Dafnakis, P.; Bracco, G.; Giorcelli, E.; Mattiazzo, G. Experimental investigation of the hydrodynamic performance of the ISWEC 1:20 scaled device. In Proceedings of the NAV International Conference on Ship and Shipping Research, Trieste, Italy, 20–22 June 2018; Number 221499, pp. 551–560. [CrossRef]

32. Bonfanti, M.; Bracco, G.; Dafnakis, P.; Giorcelli, E.; Passione, B.; Pozzi, N.; Sirigu, S.; Mattiazzo, G. Application of a passive control technique to the ISWEC: Experimental tests on a 1:8 test rig. In Proceedings of the NAV International Conference on Ship and Shipping Research, Trieste, Italy, 20–22 June 2018; Number 221499, pp. 60–70. [CrossRef]
33. Pozzi, N.; Bonfanti, M.; Mattiazzo, G. Mathematical Modeling and Scaling of the Friction Losses of a Mechanical Gyroscope. *Int. J. Appl. Mech.* **2018**, *10*, 1850024. [CrossRef]
34. Sirigu, A.S.; Gallizio, F.; Giorgi, G.; Bonfanti, M.; Bracco, G.; Mattiazzo, G. Numerical and Experimental Identification of the Aerodynamic Power Losses of the ISWEC. *J. Mar. Sci. Eng.* **2020**, *8*, 49. [CrossRef]
35. Novo, R.; Bracco, G.; Sirigu, S.; Mattiazzo, G.; Merigaud, A.; Ringwood, J. Nonlinear simulation of a wave energy converter with multiple degrees of freedom using a harmonic balance method. In Proceedings of the International Conference on Offshore Mechanics and Arctic Engineering—OMAE, Madrid, Spain, 17–22 June 2018; Volumn 10. [CrossRef]
36. Genuardi, L.; Bracco, G.; Sirigu, S.A.; Bonfanti, M.; Paduano, B.; Dafnakis, P.; Mattiazzo, G. An application of model predictive control logic to inertial sea wave energy converter. In *Mechanisms and Machine Science*; Springer: Berlin/Heidelberg, Germany, 2019; Volumn 73, pp. 3561–3571. [CrossRef]
37. Vissio, G.; Valério, D.; Bracco, G.; Beirão, P.; Pozzi, N.; Mattiazzo, G. ISWEC linear quadratic regulator oscillating control. *Renew. Energy* **2017**, *103*, 372–382. [CrossRef]
38. DNV GL. OFFSHORE STANDARD DNV GL AS Position Mooring; Technical report, 2015. Available online: https://rules.dnvgl.com/docs/pdf/dnvgl/os/2015-07/DNVGL-OS-E301.pdf (accessed on 1 January 2020).
39. Pozzi, N.; Bracco, G.; Passione, B.; Sirigu Sergej, A.; Vissio, G.; Mattiazzo, G.; Sannino, G. Wave Tank Testing of a Pendulum Wave Energy Converter 1:12 Scale Model. *Int. J. Appl. Mech.* **2017**, *9*, 1750024. [CrossRef]
40. Begovic, E.; Bertorello, C.; Prpic Orsic, J. Roll Damping Coefficients Assessment and Comparison for Round Bilge and Hard Chine Hullforms. In Proceedings of the ASME 2013 32nd International Conference on Ocean, Offshore and Arctic Engineering, Nantes, France, 9–14 June 2013. [CrossRef]
41. Begovic, E.; Day, A.; Incecik, A. An experimental study of hull girder loads on an intact and damaged naval ship. *Ocean Eng.* **2017**, *133*, 47–65. [CrossRef]
42. Bencivenga, M.; Nardone, G.; Ruggiero, F.; Calore, D. The Italian data buoy network (RON). *WIT Trans. Eng. Sci.* **2012**, *74*, 321–332. [CrossRef]
43. Venugopal, V.; Davey, T.; Smith, H.; Smith, G.; Holmes, B.; Barrett, S.; Prevosto, M.; Maisondieu, C.; Cavalieri, L.; Bertotti, L.; et al. EquiMar Project: Wave and Tidal Resource Characterisation; Technical report, 2011. Available online: https://archimer.ifremer.fr/doc/00250/36152/34706.pdf (accessed on 1 January 2020).
44. ITTC. Recommended Procedures and Guidelines 7.5-02-07-03.2: Analysis Procedure for Regular Wave Tests; Technical report, 2002. Available online: https://ittc.info/media/1323/75-02-07-032.pdf (accessed on 1 January 2020).
45. ITTC. Recommended Procedures and Guidelines 7.5-02-07-03.14: Analysis Procedure od Model Tests in Irregular Waves; Technical report, 2017. Available online: https://www.ittc.info/media/8139/75-02-07-0314.pdf (accessed on 1 January 2020).
46. ITTC. Recommended Procedures and Guidelines 7.5-02-01-01: Guide to the Expression of Uncertainty in Experimental Hydrodynamics; Technical report, 2014. Available online: https://ittc.info/media/1217/75-02-02-01.pdf (accessed on 1 January 2020).
47. Begovic, E.; Bertorello, C.; Pennino, S. Experimental seakeeping assessment of a warped planing hull model series. *Ocean Eng.* **2014**, *83*, 1–15. [CrossRef]
48. Pozzi, N.; Bracco, G.; Passione, B.; Sirigu, S.A.; Mattiazzo, G. PeWEC: Experimental validation of wave to PTO numerical model. *Ocean Eng.* **2018**, *167*, 114–129. [CrossRef]



© 2020 by the authors. Licensee MDPI, Basel, Switzerland. This article is an open access article distributed under the terms and conditions of the Creative Commons Attribution (CC BY) license (http://creativecommons.org/licenses/by/4.0/).